

University of Alberta

**MEASURING EMISSIONS FROM A  
COMMERCIAL DAIRY FARM: AN INVERSE  
DISPERSION TECHNIQUE**

By

ELIZABETH H. SHADWICK, B.SC.



A Thesis

Submitted to the Faculty of Graduate Studies and Research  
in Partial Fulfillment of the Requirements  
for the Degree

Master of Science

Department of Earth and Atmospheric Science

Edmonton, Alberta  
Spring 2006



Library and  
Archives Canada

Bibliothèque et  
Archives Canada

Published Heritage  
Branch

Direction du  
Patrimoine de l'édition

395 Wellington Street  
Ottawa ON K1A 0N4  
Canada

395, rue Wellington  
Ottawa ON K1A 0N4  
Canada

*Your file* *Votre référence*  
*ISBN: 0-494-13884-X*  
*Our file* *Notre référence*  
*ISBN: 0-494-13884-X*

#### NOTICE:

The author has granted a non-exclusive license allowing Library and Archives Canada to reproduce, publish, archive, preserve, conserve, communicate to the public by telecommunication or on the Internet, loan, distribute and sell theses worldwide, for commercial or non-commercial purposes, in microform, paper, electronic and/or any other formats.

The author retains copyright ownership and moral rights in this thesis. Neither the thesis nor substantial extracts from it may be printed or otherwise reproduced without the author's permission.

#### AVIS:

L'auteur a accordé une licence non exclusive permettant à la Bibliothèque et Archives Canada de reproduire, publier, archiver, sauvegarder, conserver, transmettre au public par télécommunication ou par l'Internet, prêter, distribuer et vendre des thèses partout dans le monde, à des fins commerciales ou autres, sur support microforme, papier, électronique et/ou autres formats.

L'auteur conserve la propriété du droit d'auteur et des droits moraux qui protègent cette thèse. Ni la thèse ni des extraits substantiels de celle-ci ne doivent être imprimés ou autrement reproduits sans son autorisation.

---

In compliance with the Canadian Privacy Act some supporting forms may have been removed from this thesis.

Conformément à la loi canadienne sur la protection de la vie privée, quelques formulaires secondaires ont été enlevés de cette thèse.

While these forms may be included in the document page count, their removal does not represent any loss of content from the thesis.

Bien que ces formulaires aient inclus dans la pagination, il n'y aura aucun contenu manquant.

  
**Canada**

*Dedicated to Elsie Frances Shadwick*

# Abstract

A backward Lagrangian Stochastic (bLS) model was applied to measure  $CH_4$  emissions from a commercial dairy farm. The experimental field site was representative of a typical Canadian dairy farm in terms of animal feeding and management strategies. Methane concentrations were measured using a multi-channel tunable diode laser. Seven open path lasers and reflectors were connected to a single laser beam. This procedure was expected to reduce the error associated with drift between sensors and that associated with calibration of several individual units. It is shown that the bLS model technique can diagnose the ‘whole-farm’  $CH_4$  emission rate with confidence. Emission estimates made by means of a ‘model-free’ ratiometric computation using the tracer gas  $SF_6$  confirm the good performance of the bLS model in this situation.

A preliminary study tested the performance of a forward Lagrangian Stochastic (LS) model with respect to plume timing. By reference to a short-range tracer experiment in a neutral, horizontally-uniform surface layer, it has been shown that the LS model replicates well the timing of concentration onset and fade-off due to a transient (point) source. An algorithm to parameterise the ‘surface delays’ experienced by particles in the unresolved layer beneath the trajectory reflection height  $z_r$  was applied, but there was found to be negligible advantage in doing so.

# Acknowledgements

First and foremost I would like to thank John Wilson for his patient and supportive supervision of this program. I am very grateful for the opportunity he has given me and sincerely hope that I have been able to make the most of it. Thanks also to Tom Flesch for cheerfully letting me drop by unexpectedly with questions, and also for the company and advice down in Lethbridge. Thank you to Edward Lozowski and Paul Myers for two thoroughly enjoyable undergraduate classes in atmospheric science - I couldn't have had a better introduction. Many thanks to the agricultural-meteorology team at Agriculture Canada in Lethbridge, and to Trevor and Nathan especially. A big thank you to my friend John Postma, without whom I would certainly still be struggling with Unix, FORTRAN and perhaps even computing in general! Thanks to Jen Jackson and John Postma for the many hours of good conversation and much needed distraction. Many thanks to my uncle Brad who is always willing, though he feigns annoyance, to rescue me from computing emergencies whenever and however they arise.

I am grateful to my Mom for all the encouragement she has given me and because she has always been the first to help me when I (inevitably) needed it. I could not possibly have done this without her help. Thanks to my Dad for his guidance and interest in my work and, most importantly, for his academic example. A special thank you to both my parents for my brother William who has given me a lifetime of entertainment and support. A final thank you to Rob, who has been greatly missed, for keeping me smiling from an ocean away.

# Contents

<b>1</b>	<b>Introduction to Micrometeorological Flux Measurements</b>	<b>1</b>
1.1	Context . . . . .	2
1.2	Existing Techniques to Determine Livestock-Atmosphere Gas Fluxes .	5
1.2.1	Flux Gradient . . . . .	6
1.2.2	Eddy-Covariance . . . . .	8
1.2.3	Micrometeorological Mass Difference . . . . .	10
1.2.4	Emissions from Ruminants Using a Calibrated Tracer . . . . .	13
1.3	The Backward Lagrangian Stochastic Technique . . . . .	14
1.4	Scope of Thesis . . . . .	15
<b>2</b>	<b>Theory of Lagrangian Dispersion Models</b>	<b>17</b>
2.1	Forward Lagrangian Stochastic Model . . . . .	17
2.2	Backward Lagrangian Stochastic Model . . . . .	20
2.3	Previous Applications . . . . .	22
<b>3</b>	<b>Transient Point Source Experiment to Test Lagrangian Model</b>	<b>26</b>
3.1	Introduction . . . . .	26
3.2	The Field Experiment . . . . .	27
3.3	Forward LS Model . . . . .	31

3.3.1	Horizontal Velocity Components of the LS Model . . . . .	32
3.3.2	Surface Reflection . . . . .	32
3.3.3	Concentration Computations . . . . .	34
3.4	Results . . . . .	34
3.5	Conclusion . . . . .	42
<b>4</b>	<b>Field Experiment to Determine Dairy Farm Emissions</b>	<b>43</b>
4.1	The Experiment Site . . . . .	43
4.2	Tracer Source . . . . .	44
4.3	Methane Concentration Measurements . . . . .	46
4.3.1	Methane Lasers . . . . .	46
4.3.2	Background Concentration Measurement . . . . .	47
4.3.3	Calibration of the Gas Lasers . . . . .	48
4.3.4	Laser Positions . . . . .	51
4.4	$SF_6$ Measurements and the Sample Line . . . . .	54
4.5	Meteorological Observations . . . . .	55
<b>5</b>	<b>Data Analysis and Results: Dairy Farm Emissions</b>	<b>58</b>
5.1	Data Filtering . . . . .	58
5.2	Emission Estimates . . . . .	60
5.2.1	Backward Lagrangian Stochastic Model . . . . .	60
5.2.2	Application of the bLS Model . . . . .	60
5.2.3	Ratiometric Computation . . . . .	61
5.3	Results . . . . .	63
5.3.1	bLS Estimate of ‘Whole-Farm’ Emissions . . . . .	63
5.3.2	bLS Estimate of Artificial Source Strength . . . . .	69

<b>6 Conclusions</b>	<b>71</b>
<b>Appendix 1</b>	<b>75</b>
<b>Appendix 2</b>	<b>86</b>
<b>Bibliography</b>	<b>87</b>



# List of Tables

3.1	Observed and modelled mean concentrations over the “source on” intervals, for a reflection height of $z_r = z_0$ . Concentrations are given in ppm. Laser 1 refers to the near laser, path length = 102 m; Laser 2 refers to the far laser, path length = 213 m. . . . .	37
3.2	Observed and modelled mean concentrations, with and without the surface delay algorithm, for a reflection height of $z_r = 7z_0$ . Concentrations are given in ppm by volume. . . . .	38
4.1	Cable compensation values resulting from both the field and retrospective (R1-R4) calibrations, for all seven laser heads . . . . .	51
4.2	The fetch (nominal distances from the farm to the sensor) and path length for each of the laser heads, given in meters. . . . .	54

5.1	Farm (only) emission estimates for the Sept. 30th and Oct. 2nd releases. The second column ('Gas On') refers to an emission estimate made by subtracting the artificial methane from the total emission over the release period, the 'Gas Off' value is an estimate of emission made when no artificial gas was released. All values are given in $\text{g day}^{-1}$ . Note that the "ratiometric" estimate is based on GC sampling from an intake line, whereas the other two columns hinge on the application of the bLS to those laser detectors standing in the plume off the farm. . . . .	66
5.2	Farm (only) emission estimates based on the sample line data, comparing the bLS and the ratiometric estimates. All values are given in $\text{g day}^{-1}$ . . . . .	67
5.3	Emission estimates for the Sept. 30th and Oct. 2nd releases. All values are given in $\text{g day}^{-1} \text{ animal}^{-1}$ and the bLS estimates are within $\pm 35 \text{ g day}^{-1} \text{ animal}^{-1}$ . The RM' column gives the corrected ratiometric results. (Note: except for column RM', values differ from those of Table 5.1 only due to the different units.) . . . . .	69
5.4	Emission estimates for the Sept. 30th and Oct. 2nd releases used to deduce the bLS estimate of the source strength of the artificial methane. All values are given in $\text{g day}^{-1}$ . . . . .	70
5.5	bLS estimates for source strength of artificial methane and the average value of these. All values are given in $\text{g s}^{-1}$ . . . . .	70

6.1 Details of the laser configurations used in the bLS emission estimates. Please refer to Fig. (4.6) to see the positions of the sensors around the farm. ‘NSA’ refers to the stand-alone laser unit located in the northernmost position away from the farm complex. ‘ $C_b$ ’ refers to the atmospheric background methane concentration. The first three configurations listed for the September 30th release, and the first two listed for the October 2nd release were used to obtain the results listed in Chapter 5. . . . . 86

# List of Figures

1.1	A schematic representation of (on the left) mean concentration as a function of height and (on the right) mean vertical flux as a function of height, assuming a uniform surface source extending a finite distance upwind, in the lower atmosphere. Note that the scale on the height axis is different for each plot. In the atmospheric surface layer, flux is constant with height up to a height of the order of (nominally) $1/100^{th}$ of the fetch of the source. . . . .	7
1.2	A schematic representation of the experimental configuration of Harper et al. (1999) for the MMD method. Measurements of $CH_4$ were made at four heights along each boundary. From measurements of wind direction, $\mathbf{u}$ was resolved into components $U_0$ normal to boundaries 2 and 4, and $V_0$ normal to boundaries 1 and 3. . . . .	11
1.3	A schematic representation of the set up used in the experiment of Desjardins et al., (2004) with multiple laser paths at one location downwind of the source. . . . .	12

2.1	A schematic representation of the bLS technique to estimate the emission rate $Q$ (following Flesch et al. 2004). The average concentration $C$ is measured at a point $M$ downwind from the source. $Q$ is calculated using the upwind trajectory touchdowns within the source where $w_0$ is the vertical velocity at the touchdown. . . . .	22
3.1	Setup of simulation, defining the $x, y$ axes, the orientations of the (selected) laser, and the direction of the mean wind. . . . .	28
3.2	Concentration time series as recorded by the nearer sensor at a nominal distance of about 24 m from the point source with path length = 102 m.	30
3.3	Concentration time series as recorded by the far sensor, at a nominal distance of about 45 m from the source with path length = 213 m. . .	30
3.4	Comparison of observed trace of (ensemble- and line-averaged) concentration with corresponding prediction of the LS model, for the nearer laser (nominally 24 m from the source, with path length 102 m) with trajectory reflection height $z_r = (z_0, 7z_0)$ . The source was turned on $t = 1$ min, and turned off $t = 6$ min . . . . .	35
3.5	Comparison of observed trace of (ensemble- and line-averaged) concentration with corresponding prediction of the LS model, for the far laser (nominally 45 m from the source, with path length 213 m) with trajectory reflection height $z_r = (z_0, 7z_0)$ . . . . .	36
3.6	Comparison of ensemble-averaged observed concentration with LS model concentration for the nearer laser (nominally 24 m from the source, with path length 102 m) with and without the surface delay algorithm with a reflection height of $z_r = 7z_0$ . The label LS_SD refers to the LS model with the application of the surface delay algorithm. . . . .	38

3.7	Comparison of ensemble-averaged observed concentration with LS model concentration for the far laser (nominally 45 m from the source, with path length 213 m) with and without the surface delay algorithm with a reflection height of $z_r = 7z_0$ . The label LS_SD refers to the LS model with the application of the surface delay algorithm. . . . .	39
3.8	Comparison of plume fade-off for the nearer laser (nominally 24 m from the source, with path length 102 m) with and without the surface delay algorithm with reflection height $z_r = (z_0, 7z_0)$ . . . . .	40
3.9	Comparison of plume fade-off for the far laser (nominally 45 m from the source, with path length 213 m) with and without the surface delay algorithm with reflection height $z_r = (z_0, 7z_0)$ . . . . .	41
4.1	Configuration of experimental site . . . . .	44
4.2	One of the seven laser heads used with the multi-channel unit. The scope was used to aim the laser at the retro reflector located approximately 350 m away. . . . .	47
4.3	This 3 m tube was used with a standard test gas in the field calibration.	49
4.4	Example of plot used to obtain a cable compensation value with the field calibration. The y-axis is the reported ppm value of the test gas (405 ppm $CH_4$ with a 3 m tube), the dashed line indicates the true value of 1215 ppm. The $cc$ value obtained from this calibration was $cc = 1.09$ . It can be seen qualitatively that the value closest to the true concentration is obtained using a $cc$ value of 1.1. . . . .	50
4.5	The trailer housed the multi-channel unit, and the laptop computer. .	52

4.6	Locations of laser heads around the farm. The numbers 1-7 refer to the channels that were used with those laser heads, the laser labelled ‘NSA’ (North Stand-Alone) refers to the stand-alone unit used at the northernmost location. . . . .	53
4.7	An open-path laser was run parallel to the sample line, and was used to check the calibration of the laser against the values of concentration obtained through GC analysis. . . . .	55
4.8	Meteorological measurements were made with a 3-D sonic anemometer which was mounted on the tower shown here. . . . .	56
5.1	The figure on the left depicts an example of good source area coverage, while the figure on the right depicts an example of bad source area coverage which would not be included in the emission estimate. The light grey area represents the ‘plume’ of computational particles. Interaction of these particles with the source area results in a dark grey colour on the source. In the image on the left, the source is almost entirely covered in particles, while in the figure on the right most of the source area has not had any interaction with the plume of computational particles. The WindTrax software displays the sensing laser as a line joining “start” and “end”. . . . .	59
5.2	The concentration time series recorded during the field experiment on Sept. 30th. The artificial methane release began at 12:00 and ended at 12:50. . . . .	63

5.3	The concentration time series recorded during the field experiment on Oct. 2nd. The first artificial methane release period began at 13:10 and ended at 13:50, and the second release period began again at 14:30 and ended at 15:15. . . . .	64
5.4	The emission time series resulting from the bLS model computation, using the concentration data from the Sept. 30th release period (gas on from 12:00 to 12:50). On the second y-axis is concentration in ppm. The square wave indicates the source strength of the added methane.	65
5.5	Examples of (5-min) period of the bLS model run using the GC data and the sample line location as inputs. On the left is the configuration of the sample line for September 30th, and on the right the configuration for October 2nd. . . . .	68



# List of Nomenclature

$a_i$	drift term in Langevin Equation
$\bar{a}$	mean quantity
$a'$	deviation from mean
$b_{i,j}$	diffusion term in Langevin Equation
$c$	concentration
$C_0$	empirically determined constant
$C_b$	atmospheric background concentration
$cc$	calibration coefficient
$C_L$	line-average concentration
$F$	surface flux
$g$	gravitational constant
$g_a$	eulerian probability density function
$k_v$	von Karman's constant
$L$	Monin-Obukhov length
$N_p$	number of particles
$Q$	emission rate
$T$	air temperature
$u$	along-wind component of velocity vector
$u_*$	friction velocity
$v$	cross-wind component of velocity vector
$w$	vertical component of velocity vector
$\overline{w'T'}$	mean vertical flux density of sensible heat
$x$	along-wind cartesian co-ordinate
$y$	cross-wind cartesian co-ordinate
$z$	vertical cartesian co-ordinate
$z_0$	surface roughness length
$z_r$	trajectory reflection height
$\epsilon$	turbulent kinetic dissipation rate
$\phi$	stability parameter

$\phi_h$	stability function for Heat
$\rho$	air density
$\sigma_u$	streamwise velocity standard deviation
$d\xi_j$	Gaussian random increment in Langevin Equation
bLS	backward Lagrangian stochastic
$CH_4$	methane
$CO_2$	carbon dioxide
EC	eddy-covariance
ERUCT	estimates from ruminants using a calibrated tracer
FG	flux gradient
GC	gas chromatography
GPS	global positioning system
IHF	integrated horizontal flux
LS	Lagrangian stochastic
MMD	micrometeorological mass difference
$N_2$	nitrogen gas
$NH_3$	ammonia
PDF	probability density function
ppm	parts per million by volume
ppmm	parts per million metres
ppt	parts per trillion by volume
RM	ratiometric
$SF_6$	sulphur-hexafluoride
TKE	turbulent kinetic energy

# Chapter 1

## Introduction to Micrometeorological Flux Measurements

Without accepting the claims that the putative recent climatic changes are entirely anthropogenic, attention may still be given to the aim of reducing atmospheric greenhouse gas concentrations. In order to reduce Canadian greenhouse gas emissions in the context of the very recently implemented though as yet grossly unplanned for Kyoto accord, it will be necessary to have reasonably accurate ways of determining the magnitude of these emissions. This research assesses the effectiveness of applying a backwards Lagrangian Stochastic technique to the measurement of methane emissions from a dairy farm. Successful application of this technique has the potential to become a significant tool for estimating and (perhaps) mitigating methane emissions from agricultural sources. These are of particular importance to Canada as agricultural sources account for 16% of the nation's global greenhouse gas contribution (Desjardins et al. 2001).

## 1.1 Context

Methane is a greenhouse gas second in importance only to carbon dioxide. Like  $CO_2$ , methane ( $CH_4$ ) traps infrared radiation that would otherwise escape into space. Methane molecules can absorb (infrared and ultraviolet) radiation, causing the molecule to vibrate. Eventually, the vibrating molecule will emit the radiation again, and it will likely be absorbed by yet another greenhouse gas molecule. This absorption-emission-absorption cycle impedes the escape of thermal radiation and in effect acts to keep heat near the earth's surface. An increased concentration of greenhouse gas molecules in the atmosphere leads to a reduction in the mean free path of emitted photons of a particular wavelength. This reduction in the mean free path is the corollary of a greater probability of absorption and re-emission, and leads to a warming in the atmosphere because the effective 'resistance' for upward transfer of energy in radiant form is increased.

Like carbon dioxide, methane has become something of a household term of late; we have grown accustomed to reports of increasing concentrations of greenhouse gases in the atmosphere. The majority of the increase in methane since pre-industrial times, as determined from ice cores and atmospheric records, is due to the increase in emissions from anthropogenic activity (Weubbles & Hayhoe 2001). Atmospheric methane concentrations have more than doubled since the beginning of the industrial age (Weubbles & Hayhoe 2001) and the steady growth in  $CH_4$  concentration makes an important direct contribution to the enhanced greenhouse effect. Over a one hundred year period, 1kg of  $CH_4$  has the same warming potential as 21 kg of  $CO_2$  (Desjardins et al. 2001). Stated alternatively, molecule for molecule  $CH_4$  traps 21 times the amount of the sun's heat in the atmosphere as does  $CO_2$  (Pearce 1989). A standard measure of this forcing, called "radiative forcing", is the change,

$\Delta Q$ , in (global mean) net radiation at the tropopause attributable to the increase in concentration of the gas in question. This measure allows direct comparison of forcing agents, whereas before the mid-1980's nearly all estimates of the greenhouse effect were given as temperature changes, that is, responses of the system (Charlson 1999). As introduced above, the human-induced increases in global atmospheric concentrations of  $CH_4$ , (and  $CO_2$ , several chlorofluorocarbon (CFC) gases, and  $N_2O$ ) have led to an enhancement of  $2.6 \text{ W m}^{-2}$  in the greenhouse effect, or the equivalent of more than 1% of the mean annual incoming absorbed solar radiation (Charlson 1999). The atmospheric concentration of  $CH_4$  rose by 0.6% per year during the decade 1984 – 1994 and  $CH_4$  accounted for about 20% of the enhancement of global radiative forcing due to perturbation in the atmospheric concentration of greenhouse gases (Houghton et al. 1995). Thus although the yearly increase in  $CO_2$  is 100 times larger than that of  $CH_4$ , methane plays a sizable role.

One anthropogenic methane source is of particular interest here: emission from domestic ruminants. Domestic ruminants account for an estimated 25% of global anthropogenic methane emissions (Weubbles & Hayhoe 2001). In Canada 15 – 20% of total greenhouse gas emissions come from agriculture\*, and roughly 40% of this agricultural emission is in the form of methane (Desjardins et al. 2001). Microbial processes taking place in the rumen of livestock, such as cattle and sheep, produce methane gas by a process termed 'enteric fermentation'. Methane produced in the digestive tract and rumen is then absorbed into the blood stream, subsequently released in the lungs, and finally exhaled through the nose and mouth of the animal (Murray et al. 1976).

---

\*This estimate encompasses all sources of GHG emission including confined livestock operations, free ranging animals, transport and slaughter of livestock, animal waste, crop production and transport, etc.

It has been suggested (Tol et al. 2003) that in the short term, reducing methane emissions may provide an opportunity to limit the cost of climate control. In Canada, agriculture is a sector that is federally and provincially monitored, making it ‘controllable’ and an attractive candidate for the testing and application of mitigation strategies. One such mitigation approach is the improvement of livestock feeding and grazing regimes (Desjardins et al. 2001; Boadi et al. 2004), which has the potential to reduce the amount of methane emitted from enteric fermentation, per unit of milk or meat production.

Boadi et al. (2004) found that the addition of fats to the traditional feedlot diet given to cattle produced a significant reduction in the amount of methane emitted by the animals. Their experiment compared the  $CH_4$  emission rates from cattle fed one of two closely monitored diets. One test group was fed a diet with a low ratio of forage (whole-plant barley) to grain, and the other group was fed a diet with a high ratio of forage to grain and containing whole sunflower seeds. A decrease of approximately 20% in the daily per-animal production of  $CH_4$  was observed in the group of animals fed the high forage:grain and sunflower seed diet throughout the course of the 5 month study. In a similar experiment in which canola oil was added to the animals’ diet, Mathison (1997) found that the daily per-animal  $CH_4$  production was reduced by 33% for the duration of the experiment, which lasted several months. This depression of  $CH_4$  production is attributed to the addition of dietary fat to the animals’ feed. Long chain fatty-acids are largely non-fermentable and somehow serve to decrease the amount of methane generated in the rumen of the animal (Boadi et al. 2004).

Manipulation of feeding strategies evidently has the potential to lower  $CH_4$  emissions from domestic ruminants. However, these strategies have yet to be implemented

on a large scale; at the moment the outcome of diet manipulation is uncertain in terms of its applicability and cost effectiveness. Any measures that promise a reduction in  $CH_4$  emission from agricultural sources will require validation in real farm settings. Under the United Nations Framework Convention on Climate Change (UNFCCC) reporting obligations of national greenhouse gas inventories also require emission verification. Measurement techniques able to deliver this verification must therefore be developed.

## 1.2 Existing Techniques to Determine Livestock-Atmosphere Gas Fluxes

Quantifying the greenhouse gas emissions from various agricultural sources has received a great deal of attention over the last few years. Several techniques have been applied to this problem and still others are being developed. In the following section those measurement techniques which have been applied to quantify the amount of methane emission from ruminants, either confined in barns and pens or in fenced paddocks, will be discussed. The suitability of these methods for application at the farm scale will be evaluated, the goal of which is the justification of the choice of the Lagrangian Stochastic approach which was applied in this study. Please note that most of the techniques to be surveyed have had widespread application by micrometeorologists during several decades for the estimation of land-surface-atmosphere fluxes, such as the latent heat flux (evapotranspiration) or photosynthesis<sup>†</sup>.

---

<sup>†</sup>For more detailed reviews of micrometeorological flux measurements see Denmead and Raupach (1993), and for the case of water vapour specifically see Brutsaert (1982).

### 1.2.1 Flux Gradient

A Flux-Gradient (FG) technique was applied by Laubach and Kelliher (2005) to determine the methane emission rate from a herd of grazing dairy cattle within a fenced paddock several square-kilometres in extent. A critical approximation is to assume that the animals can be regarded as constituting effectively a spatially uniform source of gas, such that the measuring instruments can be regarded as being immersed in a ‘constant flux layer’ (Fig.(1.1)). A similar approach had been used by Judd et al. (1999) to estimate the emission of methane from grazing sheep.

The FG technique determines the vertical flux of a gas, ( $F^{FG}$  with the superscript ‘FG’ referring to Flux-Gradient), in this case  $CH_4$ , at some height  $z$  as the product of the mean concentration gradient at  $z$  and the turbulent diffusivity of the gas<sup>‡</sup>. The concentration gradient is approximated by a finite difference in mean concentration between two measurement heights,  $z_1$  and  $z_2$ , as  $\Delta\bar{c}/\Delta z$  (where  $\Delta z = z_2 - z_1$ ). The gas diffusivity is computed from similarity theory (K-theory) using the friction velocity  $u_*$  and the empirical stability function for heat  $\phi_h$  (Laubach & Kelliher 2005). The gas flux is then given by

$$F^{FG} = -\frac{k u_* z}{\phi_h(z/L)} \frac{\Delta\bar{c}}{\Delta z} \quad (1.1)$$

where  $z$  is the intermediate height between  $z_1$  and  $z_2$ ,  $k = 0.4$  is the von Karman constant, and  $L$  the Monin-Obukhov length. For a finite source area the vertical flux of a gas  $F^{FG}$  depends on height (Fig.(1.1)). To account for this limitation of the FG technique, it is required that  $z_1$  and  $z_2$  both fall within the constant flux layer, and in effect this demands a long fetch of uniform source upwind of the flux tower.

To obtain the gas flux density within the source area, a dimensionless weighting

---

<sup>‡</sup>Mean quantities will be represented by an over-line eg. the cup windspeed  $\bar{u}$ . The duration of averaging is typically 15 – 60 minutes.



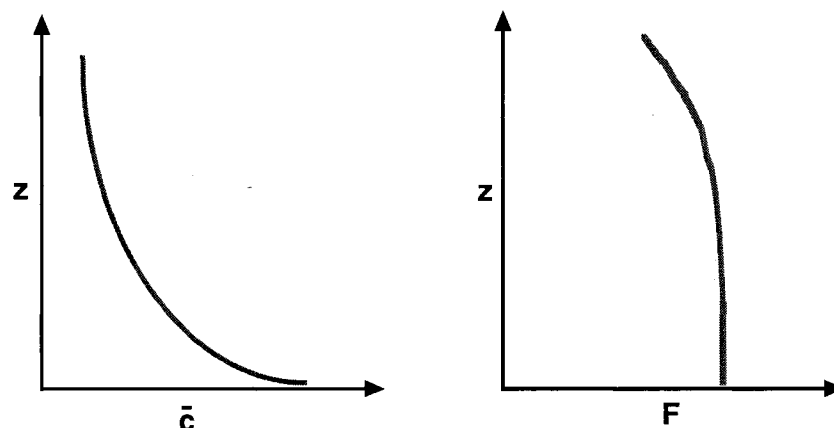


Figure 1.1: A schematic representation of (on the left) mean concentration as a function of height and (on the right) mean vertical flux as a function of height, assuming a uniform surface source extending a finite distance upwind, in the lower atmosphere. Note that the scale on the height axis is different for each plot. In the atmospheric surface layer, flux is constant with height up to a height of the order of (nominally)  $1/100^{th}$  of the fetch of the source.

factor  $S^{FG}$  is introduced (Laubach & Kelliher 2005). The emission from the source  $Q^{FG}$  (per animal) is then computed using

$$Q^{FG} = \frac{AF^{FG}}{NS^{FG}}, \quad (1.2)$$

where  $A$  is the source area, and  $N$  is the number of animals contained therein.

Although in both the Judd et al. and the Laubach/Kelliher experiments emission estimates were found to be in agreement with those obtained by other means, disadvantages of the flux-gradient method were reported. Laubach and Kelliher (2005) found that the similarity assumptions that underlie the FG method were incompatible with the limited source area they used - a fenced paddock containing grazing dairy animals. In the application of this technique to grazing sheep Judd et al. (1999) cite the disadvantage that measured mean concentrations of  $CH_4$  are, in some atmospheric conditions, near to the detection limit of the instruments used to measure

them. It has been suggested by Desjardins et al., (2004) that the flux-gradient approach requires too large a test area to be practically applicable to many ‘on-farm’ situations.

### 1.2.2 Eddy-Covariance

Eddy-covariance is another technique used to estimate the mean vertical flux of atmospheric components, and it represents the most direct or fundamental micrometeorological flux measurement method. This technique is commonly employed to estimate the surface flux of latent heat and of  $CO_2$  (see Brutsaert 1982, Hsieh et al. 1997, Werner et al. 2000). Like all flux measurement techniques, eddy-covariance relies on several assumptions about the lower atmosphere, and the terrain in which it is applied. A useful framework for discussion of flux measurements is provided by the principle of mass conservation, in mathematical form.

In the lower atmosphere the conservation of the mass of a particular component with concentration  $c$  is expressed

$$\frac{\partial c}{\partial t} = -\frac{\partial}{\partial x}uc - \frac{\partial}{\partial y}vc - \frac{\partial}{\partial z}wc = -\nabla \cdot \mathbf{F}, \quad (1.3)$$

where  $t$  is time,  $c$  is instantaneous concentration,  $u, v, w$  are the three components of velocity, and  $\mathbf{F} = \mathbf{uc}$  is the (vector) flux<sup>§</sup>. The molecular diffusion term has been neglected as it is assumed to be much smaller than the other terms in Eq.(1.3). Writing variables as the sum of the mean and fluctuating parts ( $c = \bar{c} + c'$ ) and averaging Eq.(1.3) the mean concentration equation is

$$\frac{\partial \bar{c}}{\partial t} = -\frac{\partial}{\partial x} (\bar{u} \bar{c} + \overline{u'c'}) - \frac{\partial}{\partial y} (\bar{v} \bar{c} + \overline{v'c'}) - \frac{\partial}{\partial z} (\bar{w} \bar{c} + \overline{w'c'}) = -\nabla \cdot \bar{\mathbf{F}}, \quad (1.4)$$

---

<sup>§</sup>The flux is defined as the mass of the quantity of interest passing normal to a unit area per unit time.

where the mean vector flux of mass is

$$\bar{\mathbf{F}} = (\bar{u} \bar{c} + \overline{u'c'}, \bar{v} \bar{c} + \overline{v'c'}, \bar{w} \bar{c} + \overline{w'c'}) . \quad (1.5)$$

The separable part  $(\overline{u'c'}, \overline{v'c'}, \overline{w'c'})$  is the vector constituting the turbulent, or eddy flux. Now assuming that the mean flow is stationary, horizontally homogeneous, and traversing a flat uniform surface, and that the source uniformly releases this entity, at a rate  $Q$ , one can eliminate the  $x$  and  $y$  and  $t$  derivatives. The average of Eq.(1.3) is then

$$0 = \frac{\partial}{\partial z} (\bar{w} \bar{c} + \overline{w'c'}) . \quad (1.6)$$

If one assumes that since  $\bar{w} = 0$  at the surface, then  $\bar{w}$  is everywhere zero<sup>¶</sup>, then Eq.(1.6) is reduced to

$$\frac{\partial \overline{w'c'}}{\partial z} = 0 \quad (1.7)$$

which implies that the vertical component of the turbulent flux measured at some indefinite distance above ground is equal to the mean surface emission rate  $Q^{EC}$  of the quantity  $c$ :

$$Q^{EC} = \overline{w'c'} , \quad (1.8)$$

where the superscript 'EC' is for eddy-covariance.

The eddy covariance technique is very simple in theory, but in many circumstances quite difficult to put into practice. A major problem for some gases has been the unavailability of sufficiently fast instruments to measure the fluctuating signals. Unless an instrument has a sufficiently fast response to resolve the fastest eddies contributing to the turbulent flux, this portion of the flux will not be recorded. In addition, in a situation involving animals that are free to move around, the flow is disturbed by the presence and movement of the source (the animals) making the assumption that

---

<sup>¶</sup>in fact this is implicit in the continuity equation, which in the given conditions reduces to  $\frac{\partial \bar{w}}{\partial z} = 0$

$\bar{w} = 0$  less reasonable. The eddy covariance method, like the flux-gradient technique, also requires too large a source area to be of practical use in an ‘on-farm’ setting, and is used predominantly over large, flat, uniform source areas.

### 1.2.3 Micrometeorological Mass Difference

Another technique, known as the micro-meteorological mass difference (MMD) method, has been developed to estimate emissions by determining *horizontal* fluxes, as opposed to the vertical fluxes which are determined using the FG and EC techniques, that are suitable for smaller scale measurements. Harper et al. (1999), Leuning et al. (1999), and Desjardins et al. (2004) have employed this technique to calculate emissions from artificial sources and from animals in small, bounded areas. Net emissions are calculated from the difference in the total along-wind flux of  $CH_4$  upwind and downwind from the test area. Presuming the set-up shown in Fig.(1.2), the relationship between the source strength  $Q$  and the fluxes across side boundaries (1 – 4) is

$$Q^{IHF} A = \int_{z=0}^{\infty} [\bar{u} \bar{c} + \overline{u'c'}]_2^4 dz + \int_{z=0}^{\infty} [\bar{v} \bar{c} + \overline{v'c'}]_1^3 dz, \quad (1.9)$$

where the label ‘IHF’ is for integrated horizontal flux and where the area enclosed is  $A = (y_3 - y_1) (x_4 - x_2)$ .

In both Harper et al. (1999) and Leuning et al. (1999) the mean horizontal flux was determined as the product of mean windspeed and mean concentration, ignoring terms in the streamwise eddy flux<sup>||</sup>. The latter term, sometimes called the ‘diffusive term’, has sometimes been approximated (on the basis of theory and experiment)

---

<sup>||</sup>Instantaneous windspeeds and concentrations represent the sums of time means and deviations from those means:  $u = \bar{u} + u'$  and  $c = \bar{c} + c'$ , the primes denoting the deviations from the means. The product of mean windspeed and mean concentration is then  $\overline{uc} = \bar{u} \bar{c} + \overline{u'c'}$  with the last term representing the turbulent diffusion in the upwind direction.

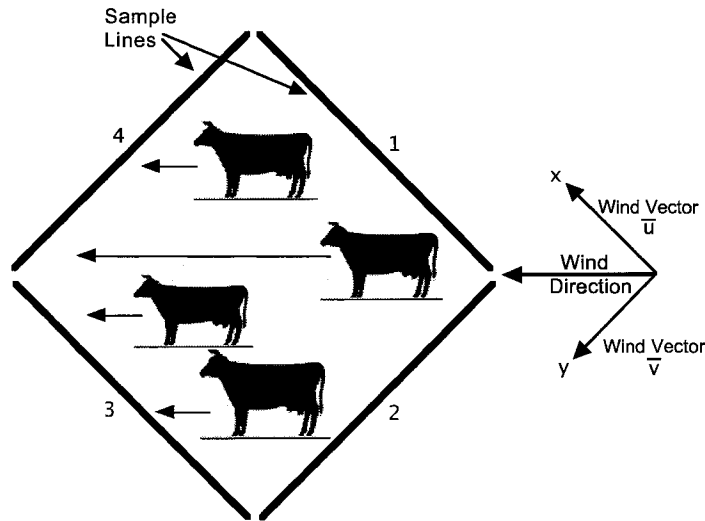


Figure 1.2: A schematic representation of the experimental configuration of Harper et al. (1999) for the MMD method. Measurements of  $CH_4$  were made at four heights along each boundary. From measurements of wind direction,  $\mathbf{u}$  was resolved into components  $U_0$  normal to boundaries 2 and 4, and  $V_0$  normal to boundaries 1 and 3.

as making up about 5 – 15% of the horizontal flux\*\* (Desjardins et al. 2004). The integral in Eq.(1.9) may then be approximated as

$$Q^{IHF} A = \int_0^\infty \bar{u}(z)[\bar{c}_4(z) - \bar{c}_2(z)]dz + \int_0^\infty \bar{v}(z)[\bar{c}_3(z) - \bar{c}_1(z)] dz. \quad (1.10)$$

In an experiment carried out by Desjardins et al. (2004), the MMD technique was simplified using sonic anemometers and open path lasers to measure mean wind-speed and mean ( $CH_4$ ) concentrations. By exploiting the long path length possible with open-path lasers, only one upwind and one (parallel) downwind boundary were considered in measuring the amount of methane emitted from an artificial source. As long as the downwind measuring path is long enough to cover the entire width of the plume of emitted gas, and the horizontal windspeed at a given height is constant across that path the MMD method can be simplified (Desjardins et al. 2004). The

---

\*\*but opposes the  $\bar{u} \bar{c}$  flux, i.e. is negative

(integrated horizontal) flux can be calculated with:

$$Q^{IHF} = X \int_0^Z \bar{u}_n (c_{z,d} - c_{z,b}) dz = X \sum_{i=1}^M \bar{u}_{ni} (c_{z,di} - c_{z,bi}) \Delta z_i, \quad (1.11)$$

where  $X$  is the plot width,  $\bar{u}_n$  is the mean wind speed normal to the enclosure boundaries, and  $c$  is the concentration with subscripts  $d$  and  $b$  denoting downwind and background concentrations respectively,  $M$  is the number of paths or laser levels defining the profile of concentration (see Fig. 1.3).

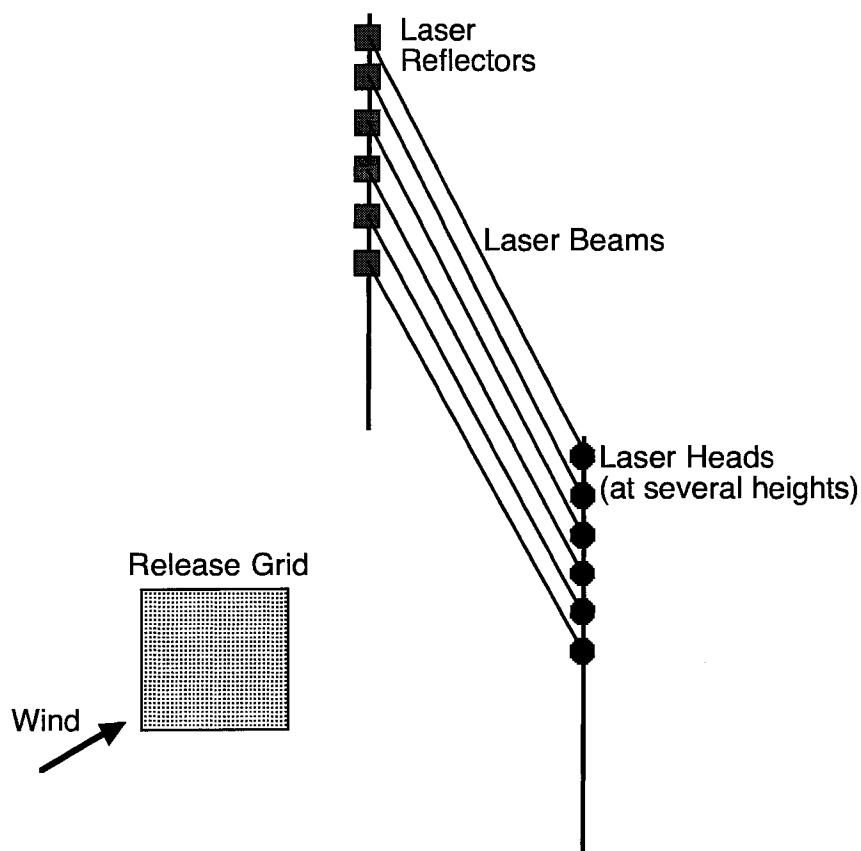


Figure 1.3: A schematic representation of the set up used in the experiment of Desjardins et al., (2004) with multiple laser paths at one location downwind of the source.

All three applications of the MMD technique that were alluded to earlier produced estimates of emission rates that were comparable with those found using other tech-

niques. Desjardins et al. (2004) concluded that the MMD method is likely the best approach to measuring emission wherever the field application allows its use. The MMD method is model free and involves fewer assumptions than other techniques. However, a number of weaknesses do exist with this technique. One practical difficulty associated with the use of this technique in an ‘on farm’ situation, (as opposed to one of artificial gas release), is the need to have unobstructed lines of sight for open-path lasers to measure concentrations. An unobstructed fetch for the measurement of the wind profile is also required - depending on the source geometry in a real farm situation these requirements may be difficult to meet. Another weakness is the difficulty of measuring small changes in concentration (i.e. the upwind-downwind differences) using the open-path lasers. The instrumentation used in the experiment of Desjardins et al. (2004) necessitates a fairly large sample size in animal trials to ensure that the emissions from the animals give rise to a downwind methane concentration well above the natural background concentration of  $CH_4$ .

#### 1.2.4 Emissions from Ruminants Using a Calibrated Tracer

The emissions from ruminants using a calibrated tracer (ERUCT) technique was developed by Johnson et al. (1994) for cattle and has since been successfully applied to sheep as well as cattle (see Lassey et al. 1997, Leuning et al. 1999, Judd et al. 1999, and Harvey et al. 2002). This technique involves placing a calibrated source of the inert tracer gas sulphur-hexafluoride ( $SF_6$ ), contained in a capsule, into the rumen of individual animals. Within the rumen, the capsule releases  $SF_6$  at a constant and known rate.

The animal’s breath is sampled unobtrusively from the nose using a yoke or a halter positioned around its neck. The breath samples are then analyzed by gas

chromatography for concentrations of both  $CH_4$  and  $SF_6$ . Assuming that both  $CH_4$  and  $SF_6$  have a similar transport pathway out of the animal, the  $CH_4$  emission rate can be estimated by assuming that the ratio of concentrations of the two gases is equal to the ratio of release rates of the two gases (Leuning et al. 1999).

Emission rate estimates from this method are typically consistent with values obtained by other means, and are generally thought to yield superior results to chamber techniques, as the animals are allowed to graze as normal throughout the experiment<sup>††</sup>. However, the variability in emission from animal to animal leaves in question the validity of scaling up from a per animal estimate to a whole herd, or whole farm, situation.

### 1.3 The Backward Lagrangian Stochastic Technique

Each of the techniques described in the previous sections has weaknesses, or disadvantages, associated with its use to quantify the amount of emission from agricultural sources at the farm scale. The eddy-covariance and flux-gradient techniques are tied to symmetry assumptions that make them incompatible with source areas of the scale that are involved in an ‘on farm’ application. On the other hand while the micro-meteorological mass difference technique may be used effectively on a smaller scale, and with a source of any geometry, beyond the rectangular configuration an integration in the crosswind direction becomes necessary (Wilson et al. 2001b) and so entails additional sampling of concentration. This greatly increases the amount of instrumentation required in the application of this technique, potentially making

---

<sup>††</sup>In other trials known as ‘chamber experiments’ animals are confined to chambers or isolated pens for the duration of the study. This confinement has a marked effect on the  $CH_4$  production of the subject, thought to be caused by the deviation from its normal routine and its isolation from the herd.



it prohibitively expensive. The ERUCT technique has no relation to source size or geometry. However, the emission estimates obtained using the internal tracer technique vary significantly from animal to animal making estimates made by scaling up to a whole farm situation uncertain. This technique is also quite invasive; whether the disruption in the test animal's routine significantly alters its  $CH_4$  production is unclear.

The backward Lagrangian Stochastic technique suffers from none of the aforementioned weaknesses, making it an attractive technique to be employed in a whole-farm scale experiment. This method has no restriction with respect to source geometry and goes unnoticed by the animals as it is carried out. It is not, however, assumption free. The gas source is assumed spatially uniform within known boundaries, and the paths of gas from source to detector are computed by a numerical model that neglects wind disturbances by the source itself. The gas transport model used here is a standard "well mixed" Lagrangian Stochastic model, appropriate to a horizontally-uniform regime of wind statistics. Such models have experienced rapid refinement in the past two decades (Wilson & Sawford 1996), and part of my thesis will constitute a further demonstration of their validity.

## 1.4 Scope of Thesis

Both forward and backward Lagrangian Stochastic models are described in detail in Chapter 2. A review of experiments in which the backward Lagrangian Stochastic technique was applied to estimate emission is given in Chapter 2 as well.

A preliminary analysis was undertaken in which the (same) Lagrangian Stochastic model was applied in a forward mode to simulate a transient source in the atmospheric surface layer. This was a means by which to gain modelling experience, and also an

opportunity to validate the Lagrangian class of model in an additional and unusual context. Chapter 3 gives the details of this preliminary modelling work and the results obtained.

In the second strand of my thesis, a field experiment was undertaken in an attempt to validate the backward Lagrangian Stochastic technique to measure emissions at the farm scale. In Chapter 4 the details of the field campaign are outlined, while the analysis of the field experiment and the results obtained are given in Chapter 5. A discussion of results and concluding remarks make up the balance of the work presented here and are found in Chapter 6.

## Chapter 2

# Theory of Lagrangian Dispersion Models

### 2.1 Forward Lagrangian Stochastic Model

The Lagrangian technique is widely regarded as the best available description for dispersion in a turbulent flow. The flexibility and computational simplicity of the Lagrangian Stochastic (LS) model are among the key advantages of this approach, particularly in cases where Eulerian approaches are less appropriate. More fundamental advantages of the LS model also exist, namely of making rational use of all known velocity statistics, and of correctly treating the non-diffusive near field of the source (Wilson & Sawford 1996).

In forward LS models, atmospheric dispersion is mimicked by computing trajectories of a large number of marked particles (or fluid elements) using the given statistical properties of the turbulent flow. The computational basis of forward LS models is a generalised Langevin equation, which follows from the assumption that particle position and velocity evolve jointly as a Markov process:

$$du_i = a_i(\mathbf{x}, \mathbf{u}, t)dt + b_{i,j}(\mathbf{x}, \mathbf{u}, t)d\xi_j \quad (2.1)$$

$$dx_i = u_i dt \quad (2.2)$$

where  $a_i$  and  $b_{i,j}$ , the drift and diffusion terms respectively, are potentially functions of  $(\mathbf{x}, \mathbf{u}, t)$ ,  $d\xi_j$  is a Gaussian random increment with zero mean and variance  $dt$ , and where  $dt$  is the time step along the trajectory (Flesch et al. 1995).

There is a constraint on the Langevin equation coefficients  $a_i$  and  $b_{i,j}$  (Thomson 1987), namely that the Eulerian probability density function (PDF)  $g_a(\mathbf{x}, \mathbf{u}, t)$  must satisfy the Fokker-Plank equation associated with Equation (2.1):

$$\frac{\partial g_a}{\partial t} = -\frac{\partial}{\partial x_i}(u_i g_a) - \frac{\partial}{\partial u_i}[a_i(\mathbf{x}, \mathbf{u}, t)g_a] + \frac{\partial^2}{\partial u_i \partial u_j}[B_{i,j}(\mathbf{x}, \mathbf{u}, t)g_a], \quad (2.3)$$

where  $B_{i,j}$  is equal to  $b_{i,j}b_{j,k}/2$  (Flesch et al. 1995). This is Thomson's (1987) well-mixed constraint.

In micrometeorology, it is normal to take the Eulerian velocity PDF  $g_a$  to be stationary, and consistency with a Kolmogorov similarity principle demands  $B_{i,j} = \frac{1}{2} C_0 \epsilon \delta_{i,j}$ . We are left with an equation that relates the model (vector) coefficient  $a_i$  to  $g_a$  (thus, to velocity statistics).

Physically, the meaning of the mathematics can be clarified by the following thought experiment. Suppose we posit a situation in which, at time  $t_0$ , tracer particles are well-mixed in position-velocity space. This would mean

$$p(\mathbf{x}, \mathbf{u}, t_0) \propto \rho(\mathbf{x}) g_a(\mathbf{x}, \mathbf{u}), \quad (2.4)$$

where  $\rho(\mathbf{x})$  is air density, and  $p(\mathbf{x}, \mathbf{u}, t)$  is the joint density function for particle location and velocity. Our tracer particles perfectly represent the motion of the air in which they are (evenly) distributed. Now assuming (in our thought experiment) that there are no sources or sinks in the flow domain, or at its boundaries, then at a later time the particles should *still* be uniformly mixed in position, and they should still be distributed in velocity space with the same distribution ( $g_a$ ) as the air. Thus, any physically acceptable model would have to have the property of ensuring (when

applied in the stated idealized case) that at a later time  $t > t_0$ ,  $p(\mathbf{x}, \mathbf{u}, t)$  remains proportional to  $\rho g_a$ . In the case where  $\rho = \text{const}$  (which we shall here assume), we are left with Eq.(2.3) or it's simplification with LHS = 0 and  $B_{i,j} = \frac{1}{2} C_0 \epsilon \delta_{i,j}$ , viz.

$$0 = -\frac{\partial}{\partial x_i}(u_i g_a) - \frac{\partial}{\partial u_i}[a_i(\mathbf{x}, \mathbf{u}, t)g_a] + \frac{C_0 \epsilon}{2} \frac{\partial^2 g_a}{\partial u_i \partial u_j} \quad (2.5)$$

Thus the well-mixed condition provides a single constraint (Eq. 2.5) on the vector coefficient  $a_i$ .

An LS model suitable for computing tracer paths in a neutrally-stratified, horizontally-homogeneous surface layer, under the approximation that the velocity PDF's for the three Eulerian velocity fluctuations are independent and Gaussian (ie. neglecting velocity correlations) and in keeping with Thomson's well-mixed constraint is

$$du_i = \frac{C_0 \epsilon u_i}{2\sigma_i^2} dt + \sqrt{C_0 \epsilon} d\xi_i \quad (2.6)$$

$$dx_i = (u_i + \bar{u}_i) dt \quad (2.7)$$

where  $u_i$  is the Lagrangian velocity fluctuation;  $\bar{u}_i = (\bar{u}(z), \bar{v}(z), 0)$  is the mean Eulerian velocity vector;  $\sigma_i^2$  is the velocity variance along coordinate direction  $i$ ; and  $d\xi_i$  is, as before, a random increment with mean zero and variance  $dt$ . An effective Lagrangian time scale can be defined by grouping terms,

$$T_L = \frac{2\sigma_i^2}{C_0 \epsilon} \quad (2.8)$$

where  $C_0$  is an empirical constant whose value depends on the specifics of the Lagrangian model, and was here assigned to  $C_0 = 3.1$  (Wilson et al., 2001b). The turbulent kinetic energy (TKE) dissipation rate is parameterised by the conventional  $\epsilon(z) = u_*^3 / (0.4 z)$  (Wilson & Sawford 1996). Equations (2.6-2.8) can be used to compute an ensemble of trajectories for particles released from a point source, while line, area, or volume sources may be handled by an appropriate summation of point

sources. The average concentration of a passive tracer due to any source can then be determined from the residence time of the tracer particles within a known sensor volume (details of this computation are given in Chapter 3).

## 2.2 Backward Lagrangian Stochastic Model

Flesch et al. (1995) introduced the backward Lagrangian Stochastic (bLS) method to calculate the dispersion of a pollutant (or tracer) from a surface area source. A key advantage of this approach is that unlike forward LS models, the computed backward trajectories are not linked to a specific source. The trajectory model for the evolution of particle position and velocity in the backwards frame of reference, in the coordinate system  $(\mathbf{x}, \mathbf{u}', t')$  with  $\mathbf{u}'_i = -\mathbf{u}_i$  and  $dt' = -dt$ , is based on a generalized Langevin equation as seen in Eq.(2.1):

$$du'_i = a'_i(\mathbf{x}, \mathbf{u}', t')dt' + b'_{i,j}(\mathbf{x}, \mathbf{u}', t')d\xi_j \quad (2.9)$$

The model coefficients  $a'_i$  and  $b'_{i,j}$ , the drift and diffusion terms must again be specified,  $dt'$  is the discrete timestep, and  $d\xi_j$  a Gaussian random increment from a population of zero mean and variance  $dt'$ . With each time step, the position of the air parcel changes by,

$$dx_i = u'_i dt' \quad (2.10)$$

and the model is iterated by applying Eq.(2.9) again. As a result of many time steps a trajectory develops. The simulation is repeated many times to represent a large number of air parcels. Obviously any interaction of these particles with the source necessitates that they must ‘touchdown’ on the source. The vertical velocity  $w$  of this contact proves to have a bearing on the contribution any touchdown makes to the concentration at the sensor (Flesch et al. 1995). When a particle touches down

on the source it makes a contribution to the surface flux from the source area with magnitude inversely proportional to its vertical velocity. With information about the wind, atmospheric conditions, and source-sensor geometry, the bLS model may be used to determine the emission rate of a given source. By consideration of units it can be seen that the ratio of source strength  $Q$  to the product of a line-average\* concentration  $C_L$  and a reference mean windspeed  $\bar{u}(h)$ , produces a dimensionless quantity,  $n$ , as given by Eq.(2.11) (Flesch et al. 1995):

$$n = \frac{Q}{C_L \bar{u}(h)}. \quad (2.11)$$

The constant  $n$  is dependent on the height  $h$  at which the reference wind speed  $\bar{u}$  is measured, on the Obukhov length  $L$ , on the surface roughness length  $z_0$ , and on the source and sensor geometry. Flesch and Wilson (1995) have shown that the left hand side of Eq.(2.11), is proportional to the sum of the reciprocals of the vertical touchdown velocities, viz.,

$$n = \frac{1}{N} \sum \left| \frac{2}{w/\bar{u}(h)} \right|. \quad (2.12)$$

$N$  is the total number of computational particles released from the sensor, i.e. the number of trajectories computed, and the vertical touchdown velocity has been normalized by the average horizontal wind speed  $\bar{u}(h)$  at the (arbitrary) reference height  $h$ . The summation ranges over all touchdowns *within the boundary of the source*. For all trajectories in which a particle touches down on the source, the vertical velocity at touchdown is recorded. These velocities are then used to calculate  $n$ , using Eq. (2.12). With the value of  $n$ , having been computed for the given conditions, measured values for the horizontal wind speed  $\bar{u}(h)$  and the line-average concentration  $C_L$  of the emitted gas, suffice to determine the source strength, or emission rate  $Q$ .

---

\*The bLS method need not refer to line-averaged concentrations, but in this thesis concentrations normally were line averages.

A separate measurement of the atmospheric background concentration of the species being measured (assuming that it occurs naturally in the atmosphere) must be made, and this concentration  $C_b$  subtracted from the line concentration  $C_L$  (see Chapter 5 for details of this computation).

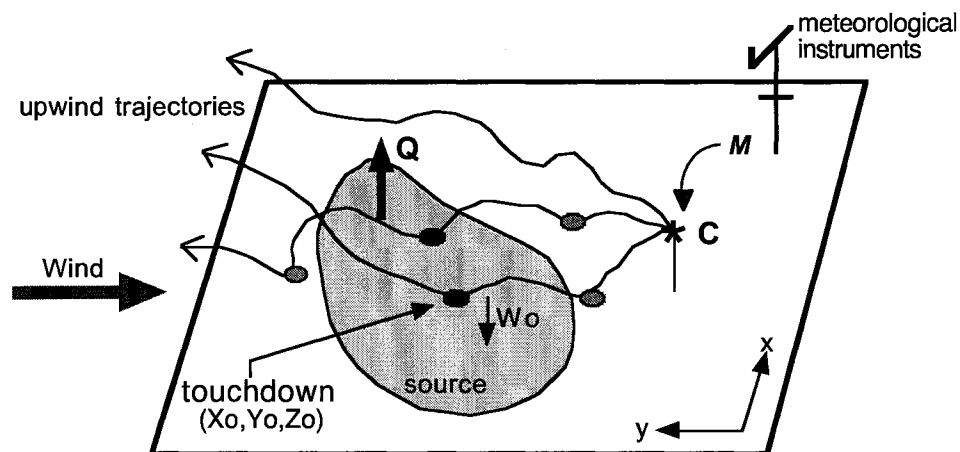


Figure 2.1: A schematic representation of the bLS technique to estimate the emission rate  $Q$  (following Flesch et al. 2004). The average concentration  $C$  is measured at a point  $M$  downwind from the source.  $Q$  is calculated using the upwind trajectory touchdowns within the source where  $w_0$  is the vertical velocity at the touchdown.

### 2.3 Previous Applications

Wilson et al. (1983) applied a Lagrangian Stochastic model to infer the rate of gas transfer to the atmosphere from a circular plot. The LS model was used to predict the shape of the concentration profile at the centre of a circular plot, which information was then used along with the roughness length and the (time-averaged) windspeed to determine the emission rate from the plot to the atmosphere. In this experiment the LS model was invoked as a means to simplify source inference; in this method the windspeed and concentration needed only to be measured at one height, at the



centre of the plot, for an emission estimate to be made<sup>†</sup>.

One of the major biogenic sources of  $CH_4$  is rice cultivation (Houghton et al. 1995), and identifying the sources and sinks of  $CH_4$  within a plant canopy is an important practical problem. Leuning et al., (2000) applied a one dimensional (height only) backward Lagrangian Stochastic model to estimate the source/sink distributions of heat, water vapour,  $CO_2$  and  $CH_4$  in a rice canopy. It was found that the bLS model produced results for the fluxes of these quantities at the top of the canopy that were in good agreement with values obtained through eddy-correlation. Denmead et al., (2000) applied the bLS approach to identify sources and sinks of similar scalars in a corn canopy. They too found that the bLS model gave flux results in good agreement with those values obtained through eddy-covariance. Both these experiments used a bLS model specific to volume sources (in plant canopies) of infinite upwind extent.

The bLS model applied in my thesis (Chapters 4 and 5) was introduced by Flesch et al. (1995) as a means to simplify experimental procedure for a broad class of source inference problems. Flesch et al. (2004) tested this method to estimate emissions from a known artificial source. It was found that the technique produced emission estimates that were in good (within 20%) agreement with the known release values. Several recommendations for the use of the bLS model to infer emission rates from an area source were put forth. One recommendation was that a line concentration sensor should be used in place of a point sensor, as this improves the accuracy with which the emission rate could be estimated. Another suggestion was that periods of extreme atmospheric stability should be removed from the data set before generating a model estimate of emission, and that periods in which the friction velocity

---

<sup>†</sup>It should be noted that in this first application of the LS model to infer emission, the (area) source had to be circular

$u_*$  is low ( $u_* \leq 0.15 \text{ ms}^{-1}$ ) should also be excluded<sup>‡</sup>.

The bLS technique has been applied by others to estimate the emission from agricultural sources. This method was applied to estimate the  $CH_4$  emission from grazing dairy cattle in New Zealand; Laubach and Kelliher (2005) compared emission estimates obtained through Flux-Gradient and Micrometeorological Mass Difference to those obtained with the bLS model. Methane concentration measurements were obtained using a flame ionisation detector within a gas chromatograph.  $CH_4$  was emitted from a herd of cattle upwind of the instruments, within a fenced paddock. The animals were moved daily and the instrument tower was moved along with them to ensure that the herd was located upwind of the sensors. Emission estimates obtained using the bLS technique were deemed to be as reliable as those obtained through other means.

The bLS technique was compared to an integrated horizontal flux (MMD) approach to estimate the  $NH_3$  emission from a manure pack by Sommer et al., (2004). Results obtained were consistent with emission values from other studies. Flesch et al., (2005) used the bLS technique to estimate the  $NH_3$  emission from a swine farm. In their set-up two open path tunable diode lasers were used to measure line-average ammonia concentrations. In this case as well, the bLS technique gave results comparable to those obtained by another method.

The field experiment to be described in Chapter 4 presents an application of the bLS model to the measurement of  $CH_4$  emissions from cattle on a commercial dairy farm, the goal of which is the validation the bLS technique in this situation. The novelty of this experiment is in the location at which it was carried out and also in the instrumentation used. The commercial dairy farm that served as a field site for

---

<sup>‡</sup>All three of these recommendations have been followed in the present application of the bLS model.

the experiment is representative of the typical Canadian dairy farm in terms of animal feeding and management strategies. The farm is surrounded on three sides by fields planted with grass and on the third side by a road. There are no other known sources of  $CH_4$  emission for several kilometres in any direction, ensuring that the methane measured results from only one collection of sources on this particular farm.

Methane concentrations were measured using a multi-channel tunable diode laser. Seven open path lasers and reflectors were connected to a single laser beam, which was expected to reduce the error associated with drift between sensors and that associated with calibration of several individual units. It is hoped that this method will provide a reliable estimate of the  $CH_4$  emission from a commercial dairy farm and may then be used as a standard by which to evaluate the dairy sector's contribution to the nation's agricultural greenhouse gas emissions.

This terminates the introductory material of my thesis. The following chapter is a novel test of the Lagrangian class of dispersion model, and can be regarded as preliminary. Chapters 4 and 5 focus on the use of such a model to deduce dairy farm emissions.

## Chapter 3

# Transient Point Source Experiment to Test Lagrangian Model

### 3.1 Introduction

There have been numerous demonstrations of the fidelity of LS models with respect to steady-state sources in a stationary atmosphere. Wilson et al. (1980) showed that the Lagrangian Stochastic method nicely simulates the observations of Project Prairie Grass\* for short range turbulent dispersion over a wide range of values of the Monin-Obuhkov length  $L$ . The Project Prairie Grass observations are regarded as the best test data for dispersion in horizontally-uniform, stratified surface layer flow. Wilson et al. concluded that the LS model provided a viable alternative to modelling dispersion problems where Eulerian methods were less appropriate.

The turbulent dispersion of aerosols above and within plant canopies is an important agricultural problem; the spread of GMO<sup>†</sup> seeds, and the effectiveness of pesticide sprays are examples of processes influenced by turbulent dispersion. An

---

\*The Project Prairie Grass (PPG) experiments are fully described by Barad (1958) and Haugen (1959). Despite the number of years that have elapsed since the experiments were carried out, the PPG observations remain the best test data for dispersion in the atmospheric boundary layer and are commonly used as a standard against which the validity of a model simulation is measured.

<sup>†</sup>Genetically Modified Organisms.

LS model was developed by Flesch and Wilson (1992) and applied to sources in a plant canopy. Under these circumstances the turbulence is still horizontally uniform, but very different from the turbulence of the surface layer flows of previous applications. The LS model was found to adequately predict mean concentrations and fluxes resulting from sources inside a non-Gaussian plant canopy flow.

In these studies, and the many others that have been performed to test the fidelity of the LS model, the tracer source was steady in time and so the resulting mean concentration field was independent of the distribution of travel times from source to detector. The primary focus of the research of this chapter was to evaluate the performance of even the simplest well-mixed (Thomson 1987) forward Lagrangian Stochastic (LS) model with respect to plume *timing*. To this end, simulations of a simple field experiment were conducted. The second objective of this research, in keeping with the focus on plume timing, was to assess the usefulness of incorporating the formulation of Wilson et al. (2001a) to parameterise the ‘surface delays’ experienced by particles in the unresolved layer beneath the trajectory reflection height  $z_r$ , and the corresponding displacements experienced by these particles<sup>‡</sup>.

## 3.2 The Field Experiment

Methane from a gas cylinder was released from a point source at height  $h_s = 0.5$  m over short grass, in a horizontally-homogeneous surface layer at the University of Alberta experimental farm, Ellerslie, Alberta (June 22, 2001)<sup>§</sup>. The gas flow rate

---

<sup>‡</sup>Submitted to ‘Boundary-Layer Meteorology’ under the title “Forward Lagrangian Stochastic Simulation of a Transient Source in the Atmospheric Surface Layer” with authorship Shadwick, Wilson, Flesch

<sup>§</sup>The field experiment was performed by Dr. John Wilson and Dr. Thomas Flesch prior to my enrolment in this program of study. The data obtained was provided for comparison with simulations which are described here.

$Q = 20 \pm 2 \text{ L min}^{-1}$  was monitored by a rotameter. Nearby, at nominal downwind distances from the source of about 24 and 45 m, two line-averaging infra-red lasers monitored methane concentration; their path lengths were respectively 102 and 213 m, and their path height  $z_L = 1.5 \text{ m}$  (Fig.(3.1)). Two 3-dimensional sonic anemometers

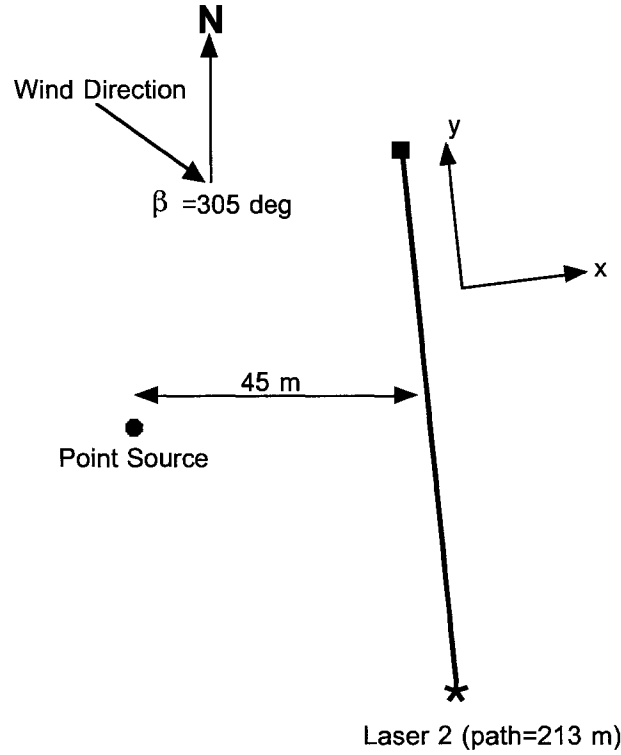


Figure 3.1: Setup of simulation, defining the  $x, y$  axes, the orientations of the (selected) laser, and the direction of the mean wind.

(Campbell Scientific CSAT3) at a height of  $z_s = 2.12 \text{ m}$  provided meteorological data averaged (during the experiment) over five-minute blocks. During a fortuitous sequence of rather constant (consecutive 5 minute) means of wind speed and direction, the source was held on and then off over alternating five minute cycles. From the sonics, during the eight “on” periods atmospheric stability was effectively neutral; the friction velocity  $u_* = 0.43 \text{ m s}^{-1}$ ; the mean “cup” windspeed  $S = \sqrt{u^2 + v^2} =$

3.95 m s<sup>-1</sup> and mean wind direction 305 deg; and the surface roughness length, which was computed by reconciling the measured friction velocity and mean windspeed according to the usual semi-logarithmic mean wind profile,

$$z_0 = z_s \exp\left(-\frac{0.4 S}{u_*}\right), \quad (3.1)$$

was  $z_0 = 0.054$  m.

The observed concentration time series from the lasers are shown in Figs.(3.2, 3.3). The time series of concentration from the laser entailed a sampling interval of order 30 seconds, each sample being an average over that duration. Thus there is no variability in the concentration trace on timescales faster than about 30 seconds. It can be seen that the preceding release does not affect the concentration over the subsequent five-minute release period, ie. each ‘on’ period may be regarded as an independent event. Thus the eight ‘on’ periods recorded during this interval of steady wind speed and direction were used to form an ensemble average against which the simulated concentration trace could be compared. The background methane concentration was deduced (independently for each of the two laser sensors) by averaging the methane concentration over the last four minutes of each ‘off’ cycle. The resulting concentrations for each of the eight ‘off’ periods were then ensemble-averaged and taken as a (constant) value for the mean background concentration. The background concentration was adjusted by a retrospective laser re-calibration so as to present a mean value of 1.9 ppm, which is consistent for the atmospheric concentration of  $CH_4$  listed (by Alberta Environment) for the day the experiment was carried out.

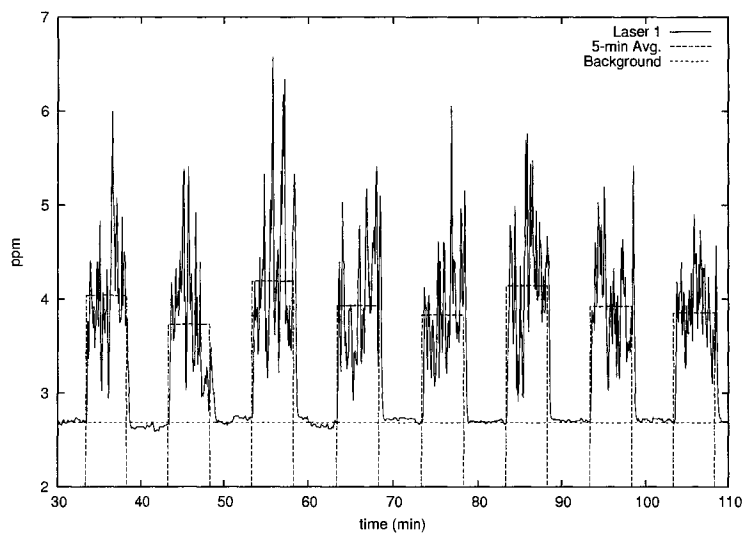


Figure 3.2: Concentration time series as recorded by the nearer sensor at a nominal distance of about 24 m from the point source with path length = 102 m.

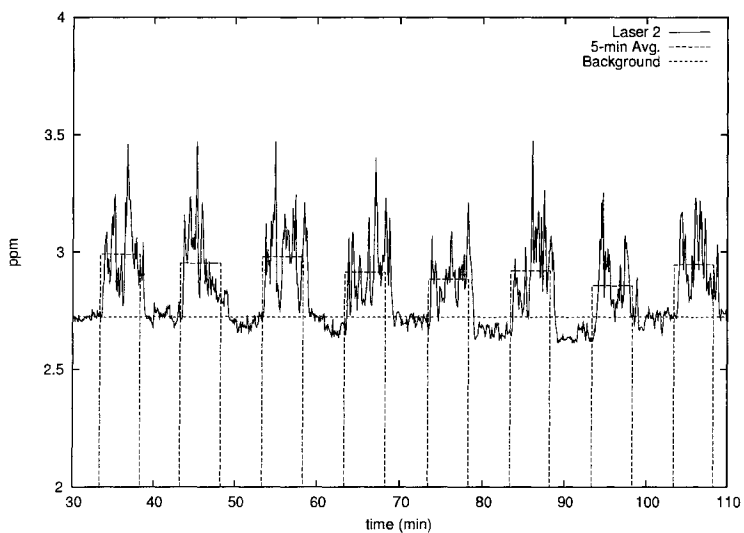


Figure 3.3: Concentration time series as recorded by the far sensor, at a nominal distance of about 45 m from the source with path length = 213 m.



### 3.3 Forward LS Model

A forward LS model suitable for computing tracer paths in a neutrally-stratified, horizontally-homogeneous surface layer was adopted and programmed in *FORTRAN* from scratch (Appendix 1). An approximation that the velocity probability density functions (PDF's) for the three (Eulerian) velocity fluctuations are independent Gaussians was made (ie. the velocity correlations were neglected). The unique well-mixed model (Thomson 1987) appropriate to these conditions is

$$du_i = \frac{C_0 \epsilon u_i}{2\sigma_i^2} dt + \sqrt{C_0 \epsilon} d\xi_i \quad (3.2)$$

$$dx_i = (u_i + \bar{u}_i) dt \quad (3.3)$$

(no summation over  $i$  in Eq. (3.2)) where  $u_i$  is the Lagrangian velocity fluctuation;  $\bar{u}_i = (\bar{u}(z), \bar{v}(z), 0)$  is the mean Eulerian velocity vector;  $\sigma_i^2$  is the velocity variance along coordinate direction  $i$ ; and  $d\xi_i$  is a random increment with zero mean and variance  $dt$ . The model timestep  $dt$  was specified as

$$dt = \mu \frac{2}{C_0 \epsilon} \min [\sigma_u^2, \sigma_v^2, \sigma_w^2] \quad (3.4)$$

with  $\mu = 0.1$ ,  $C_0 = 3.1$  (consistent with the neglect of velocity correlations: Wilson et al. 2001b),  $\sigma_u = \sigma_v = 2u_*$ , and  $\sigma_w = 1.3u_*$ . The turbulent kinetic energy (TKE) dissipation rate was parameterised by the conventional  $\epsilon(z) = u_*^3/(0.4z)$ . Equations (3.2-3.4) were used to determine an ensemble of trajectories for particles released from a point source. To mimic a release of five minutes in length,  $N_p = 100,000$  model particles were released at regular intervals throughout the simulation corresponding to a release every five seconds beginning at  $t = 2.5$  s and continuing until 2.5 s before the end of the five minute 'on' period.

### 3.3.1 Horizontal Velocity Components of the LS Model

As indicated in Figure (3.1), the model's  $y$  axis was defined to be parallel to the laser path<sup>¶</sup>, the mean wind direction  $\beta$  as the deviation-angle away from true north, and  $\beta_{mod}$  the deviation-angle away from the model's  $x$ -axis. Therefore unless the mean wind ran *perpendicular* to the (chosen) laser path (in which case in this convention the mean wind is parallel to the  $x$ -axis<sup>||</sup> from North), it was necessary that both horizontal components of the mean wind be simulated by the LS model. Following Wilson (2004), these components are

$$\begin{aligned} U(z) &= \frac{u_* \cos \beta_{mod}}{k_v} \log \left( \frac{z}{z_0} \right), \\ V(z) &= \frac{u_* \sin \beta_{mod}}{k_v} \log \left( \frac{z}{z_0} \right). \end{aligned} \quad (3.5)$$

With regard to fluctuations in horizontal velocity, due to the approximation of symmetry  $\sigma_u = \sigma_v = 2u_*$  there was no need for corresponding rotation formulae for partitioning the velocity variance.

### 3.3.2 Surface Reflection

In LS models, particle trajectories are necessarily reflected at an imposed (artificial) boundary  $z_r$  (for reflection criteria see Wilson & Flesch 1993; Thomson & Montgomery 1994). The siting of that boundary is to a large extent a matter of convenience, and so one may speed up computations by setting  $z_r \gg z_0$ , ie. by reflecting trajectories far above ground, thus obviating the need for calculations in a layer where the high turbulent kinetic energy dissipation rate  $\epsilon$  necessitates a very small time step  $dt$ . Wilson et al. (2001a) proposed an algorithm to parameterize

---

<sup>¶</sup>In the experiment the two lasers were not exactly parallel. However the Lagrangian stochastic model was run independently to compute concentration seen by each laser.

<sup>||</sup>and the mean wind direction  $\beta = 90 - \beta_{mod}$

the surface delays and corresponding spatial displacements experienced by particles descending beneath the lower boundary  $z_r$ , and the present work provided an opportunity to assess its utility. The mean delay and mean along wind displacement per reflection are

$$\bar{\tau} \approx 2.5z_r/\sigma_w \quad (3.6)$$

$$\bar{\delta} \approx \langle \bar{u}|z_r \rangle \bar{\tau} \quad (3.7)$$

where  $\langle \bar{u}|z_r \rangle$  is the height average of  $\bar{u}$  in the layer between the  $z_r$  and the surface:

$$\langle \bar{u}|z_r \rangle = \frac{u_* z_0}{k_v(z_r - z_0)} \left[ \frac{z_r}{z_0} \ln \left( \frac{z_r}{z_0} \right) - \frac{z_r}{z_0} + 1 \right]. \quad (3.8)$$

Model trials were run with two choices of reflection height,  $z_r = (z_0, 7z_0)$ . The surface delay parameterisation was applied only for trials where  $z_r = 7z_0$ . The mean displacement per reflection was  $\bar{\delta} = 2.31$  m, and the corresponding mean delay was  $\bar{\tau} = 1.69$  s. Regarding the anticipated impact of the surface delay parameterization, it should be more noticeable in its effect on the fade-away transition at the end of the on-cycle, than in its effect on the onset; this is because, by definition, the trailing edge of the concentration trace at the laser is a contribution from particles that have arrived at the laser tardily, and ipso facto, have travelled close to ground. As to whether the correction ought to have a greater impact on modelled concentration at the nearer or farther laser, this is unclear; while the significance of any one reflection (delay 1.69 s) is less significant relative to travel time as the latter increases (ie. at the downwind laser), the longer travel time causes a proportionate increase in the probable number of reflections preceding arrival.

### 3.3.3 Concentration Computations

The nearer and farther laser detectors had path lengths respectively of 102 m and 213 m. To model the concentration profile along each laser, its path was divided into 500 equally sized sample volumes with dimensions  $\Delta y = (0.204, 0.426)$  m,  $\Delta z = 0.3$  m. As we were dealing with a transient source, the model concentration was quantized then smoothed\*\* not only spatially (index  $j$ ), but also in time. The temporal ‘bin’ width  $\Delta t_b = 5$  s, and the time axis is indexed  $n$ . As the time origin  $t = 0$  was set to coincide with the source-on transition, each computational particle began its random flight at some time  $t \geq 0$ .

Whenever a particle traversed a sampling volume, the residence time contribution was computed and added to an accumulator for the appropriate location and time window (due to the small dimension of the samplers, traversal normally implied a residency time that was smaller than the timestep  $\Delta t$ ). For each sampler, the mean residence time  $\bar{t}_{j,n}$  (summed and normalised over a large number  $N_p$  of independent random flights) in location bin  $j$  and time bin  $n$ , gives the model’s estimate for the mean concentration at that time and place according to

$$C(j\Delta y, n\Delta t_b) = \frac{Q \bar{t}_{j,n}}{\Delta y \Delta z} \quad (3.9)$$

where  $Q$  kg s<sup>-1</sup> is the (physical) source strength. For the results to be shown,  $N_p = 10^5$  particles were released within each time window  $\Delta t_b = 5$  s.

## 3.4 Results

LS model results with trajectory reflection height set to  $z_r = (z_0, 7z_0)$  are compared with the observations in Figs. (3.4) and (3.5), which show that the model

---

\*\*Several model runs were used to compute an ensemble average of the concentration-transient, which was compared to the ensemble average of the 8 observational periods.

simulates the concentration at both sensor locations quite accurately (see also Table 3.1). The model concentration trace ramps on at the appropriate time, but wanes slightly early. A shorter time discretisation (ie. binning width  $\Delta t_b$ ) marginally improves the timing at the end of the release period, with the disadvantage of a much noisier estimate of  $C(t)$  throughout; using  $\Delta t_b = 5$  s represents a reasonable compromise as (for the other given choices, viz.  $N_p = 10^5$ , etc.) it results in a relatively smooth ensemble-averaged concentration at the two lasers, and furthermore provides a temporal resolution comparable to that provided by the lasers.

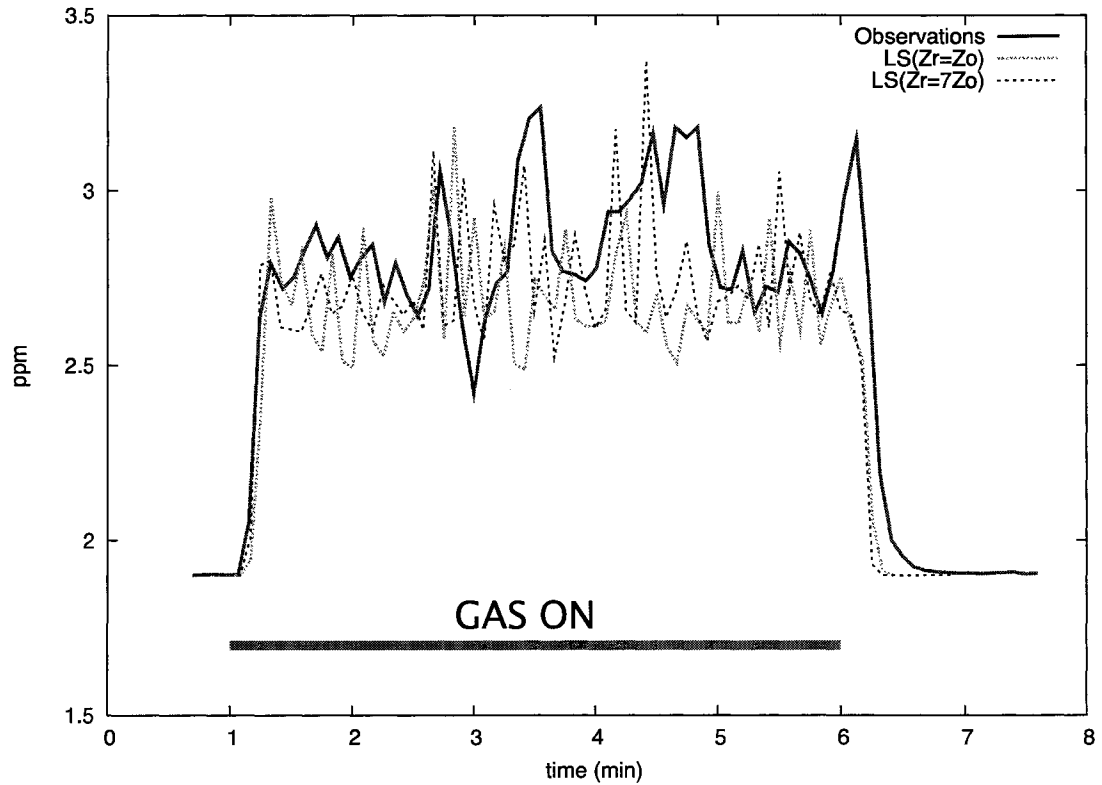


Figure 3.4: Comparison of observed trace of (ensemble- and line-averaged) concentration with corresponding prediction of the LS model, for the nearer laser (nominally 24 m from the source, with path length 102 m) with trajectory reflection height  $z_r = (z_0, 7z_0)$ . The source was turned on  $t = 1$  min, and turned off  $t = 6$  min

LS model results with the application of the surface delay parameterisation at a

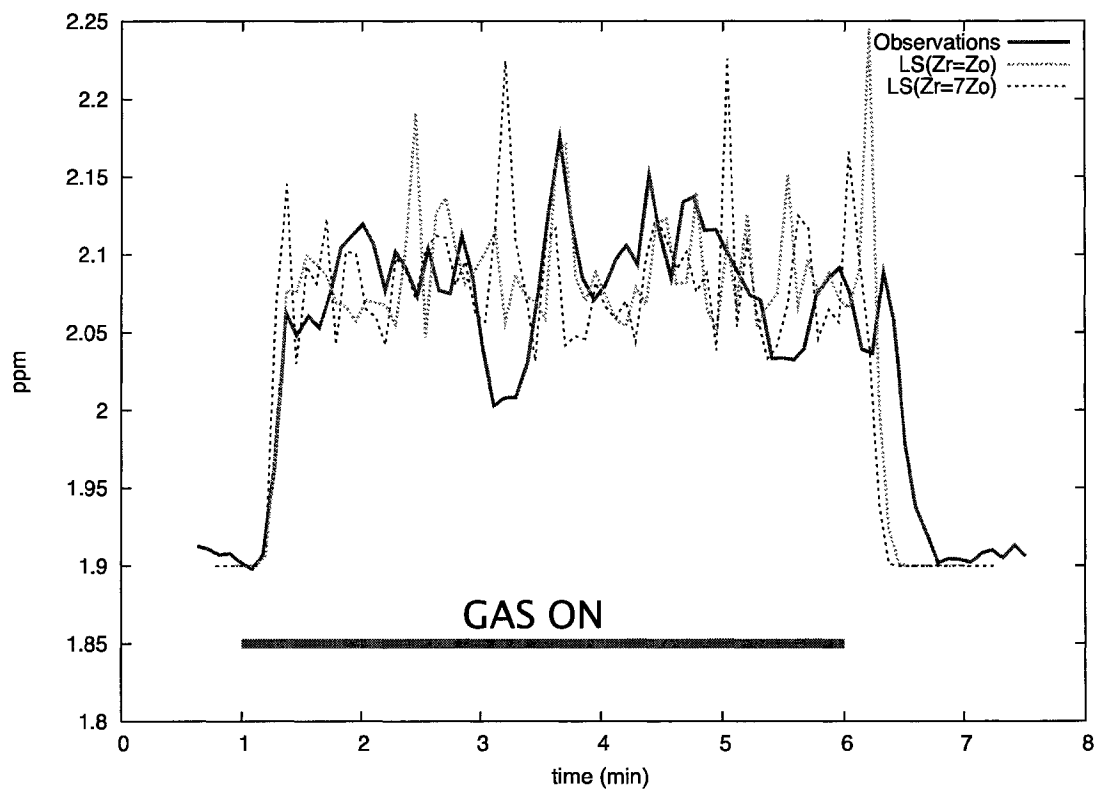


Figure 3.5: Comparison of observed trace of (ensemble- and line-averaged) concentration with corresponding prediction of the LS model, for the far laser (nominally 45 m from the source, with path length 213 m) with trajectory reflection height  $z_r = (z_0, 7z_0)$ .

reflection height of  $z_r = 7z_0$  are shown in Figs. ( 3.6 - 3.9). Even though the reflection height  $z_r = 7z_0 = 0.378$  m was quite close to the height of the source ( $h_s = 0.5$  m), the observed concentrations at both sensor locations are fairly well simulated by the LS model. The (simulated) plume arrival is again slightly premature. This timing is improved with the application of the surface delay algorithm which matches the off-timing for the case of  $z_r = 7z_0$  to that of the case where  $z_r = z_0$  for both sensor locations. The improved timing is more easily seen in Fig.(3.8) and Fig.(3.9) where the LS model and observed concentrations are compared from time  $t = 5$  min to time  $t = 6$  min.

For both sensor locations and for both choices of surface reflection height, the mean concentrations of the LS model are in good agreement with the observed mean concentrations over the 5-min period. Values of mean concentration (with and without the surface delay parameterisation for the case where  $z_r = 7z_0$ ), are summarised in Tables (3.1) and (3.2).

	Observed	LS
Laser 1	2.80	2.70
Laser 2	2.07	2.08

Table 3.1: Observed and modelled mean concentrations over the “source on” intervals, for a reflection height of  $z_r = z_0$ . Concentrations are given in ppm. Laser 1 refers to the near laser, path length = 102 m; Laser 2 refers to the far laser, path length = 213 m.

The impact of the surface delay/displacement algorithm evidently was modest on plume timing, and unimportant on mean concentration. From these results it is evident that the impact of the surface delay/ displacement algorithm on the computed concentration transient is small, at least in the case examined (very short range). As expected, the impact was greater at the trailing edge of the concentration transient

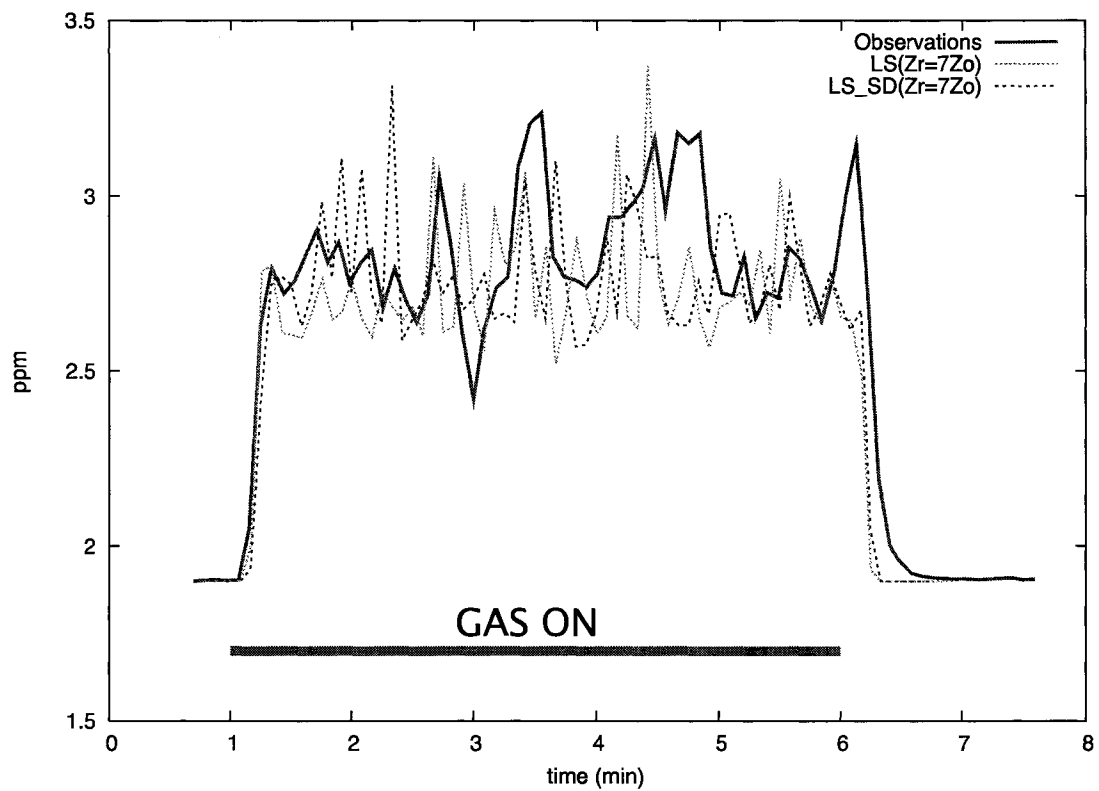


Figure 3.6: Comparison of ensemble-averaged observed concentration with LS model concentration for the nearer laser (nominally 24 m from the source, with path length 102 m) with and without the surface delay algorithm with a reflection height of  $z_r = 7z_0$ . The label LS\_SD refers to the LS model with the application of the surface delay algorithm.

	Observed	Delay	No Delay
Laser 1	2.80	2.75	2.70
Laser 2	2.07	2.09	2.08

Table 3.2: Observed and modelled mean concentrations, with and without the surface delay algorithm, for a reflection height of  $z_r = 7z_0$ . Concentrations are given in ppm by volume.



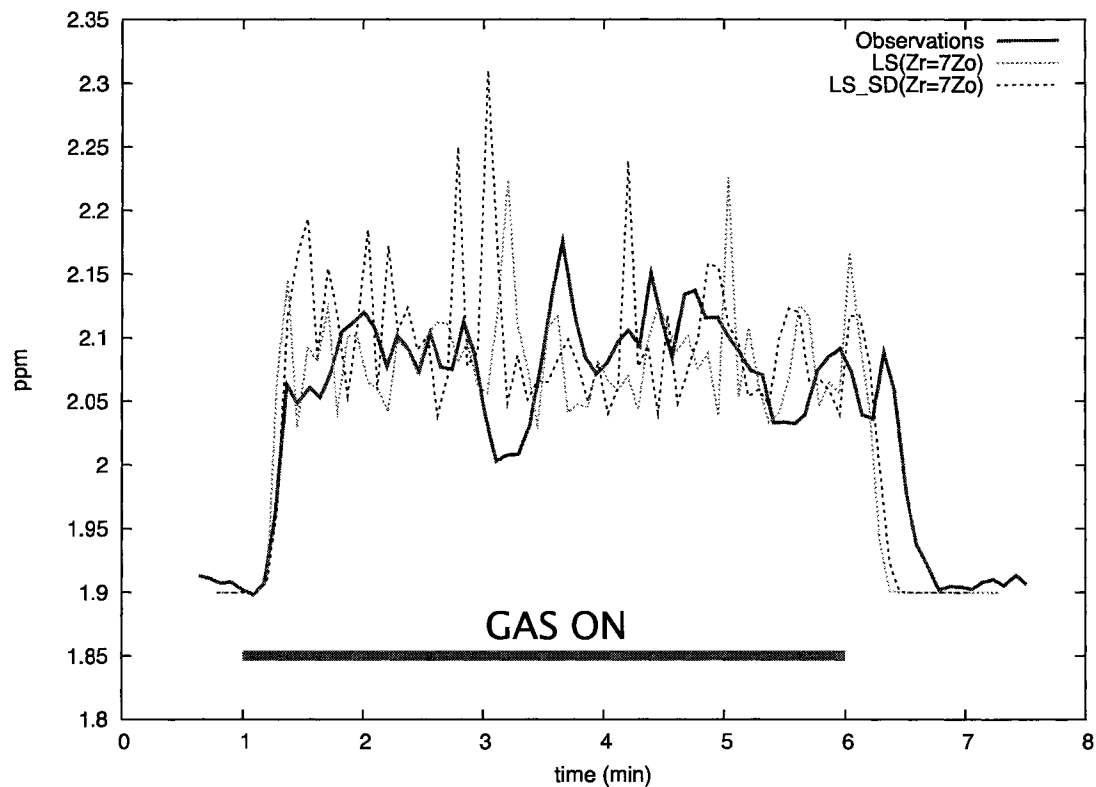


Figure 3.7: Comparison of ensemble-averaged observed concentration with LS model concentration for the far laser (nominally 45 m from the source, with path length 213 m) with and without the surface delay algorithm with a reflection height of  $z_r = 7z_0$ . The label LS\_SD refers to the LS model with the application of the surface delay algorithm.

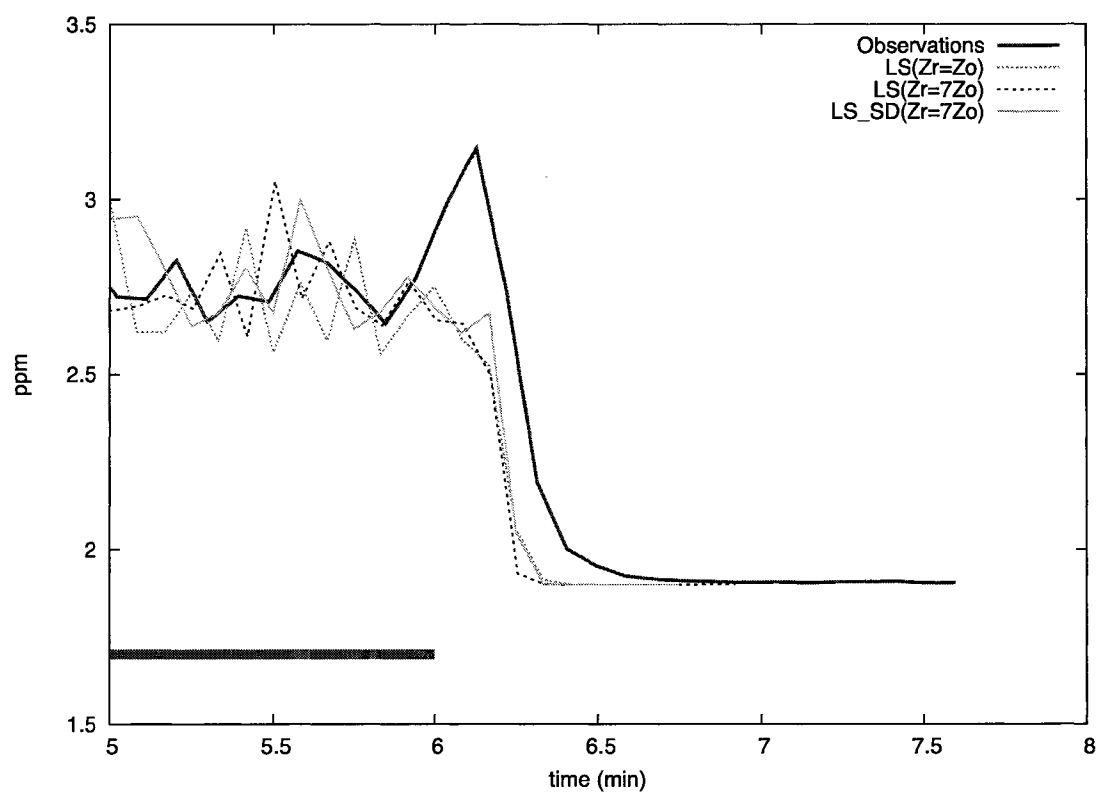


Figure 3.8: Comparison of plume fade-off for the nearer laser (nominally 24 m from the source, with path length 102 m) with and without the surface delay algorithm with reflection height  $z_r = (z_0, 7z_0)$ .

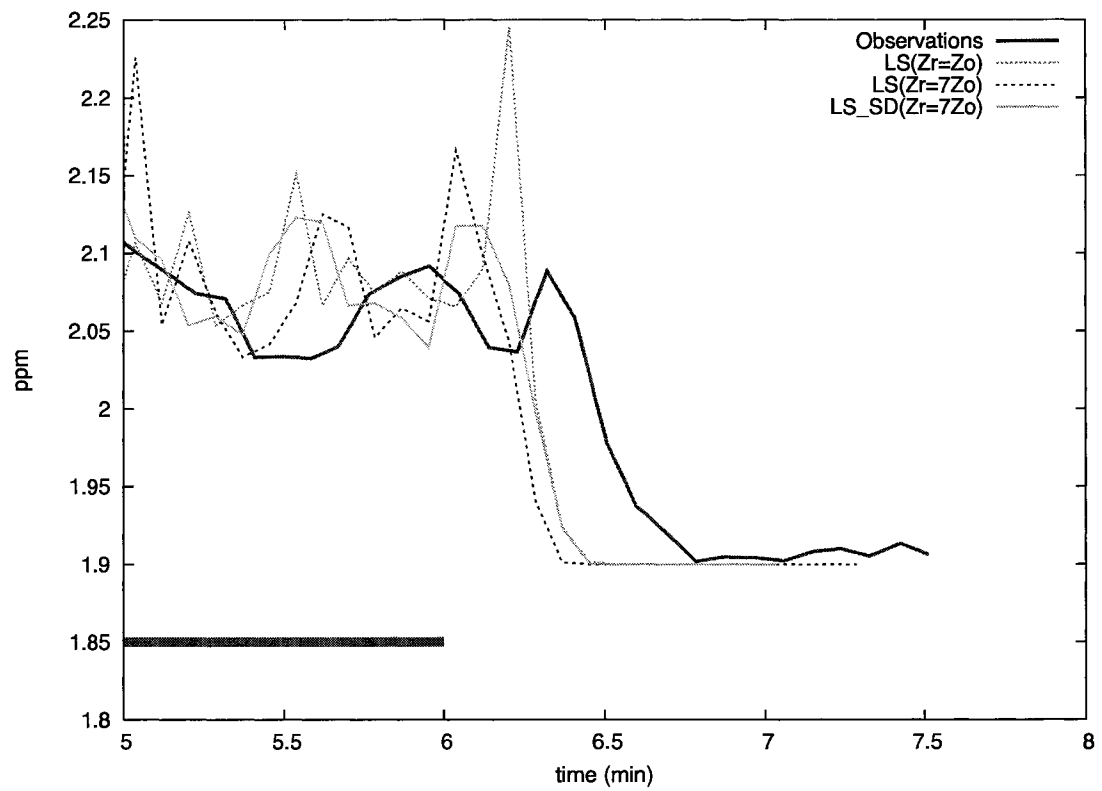


Figure 3.9: Comparison of plume fade-off for the far laser (nominally 45 m from the source, with path length 213 m) with and without the surface delay algorithm with reflection height  $z_r = (z_0, 7z_0)$ .

than at onset. It appears also to be more significant for timing of the concentration transient at the more distant of the two lasers, though this would be a weak basis to generalize that the correction should be more significant for longer range problems. In short, even with a reflection height set not very far beneath the height of the source, there seems to have been negligible penalty for neglecting the mean delay/displacement per reflection.

### 3.5 Conclusion

By reference to a short-range (order 20 - 50 m) tracer experiment in a neutral, horizontally-uniform surface layer, it has been shown that a simple LS model replicates quite well the (ensemble mean) timing of concentration onset and fade-off due to a transient source, in addition to the mean concentration during on periods. This validation represents another confirmation of the physical plausibility of the Lagrangian stochastic class of dispersion models. For the case investigated here, the quality of the LS simulations was rather insensitive to the placing of the lower reflecting boundary ( $z_r$ ), and there was found to be negligible advantage in incorporating a parameterisation for surface delays corresponding to unresolved trajectory segments beneath that height.

## Chapter 4

# Field Experiment to Determine Dairy Farm Emissions

The general aim was to evaluate the accuracy with which “bLS” could be used to estimate farm emissions. The approach taken was to set up a situation in which gas emission rates into the passing wind were *independently* known.

### 4.1 The Experiment Site

The field experiment was carried out in cooperation with the agricultural-meteorology team at the Agriculture and Agri-Food Canada research station in Lethbridge, Alberta. Methane concentration measurements were gathered at a commercial dairy farm over the course of a two week period in late September and early October, 2005. The farm was comprised of an L-shaped barn, a large open air pen located north of the barn, and a long row of open air pens adjacent to the barn and running east-west (see Fig. (4.1)). The upper part of the barn walls (on the sides of the building running north-south) were screen windows covered by curtains which opened and closed depending on the temperature inside the barn. The curtains were open during the day to allow ventilation from the barn. Along the peak of the barn roof ran open

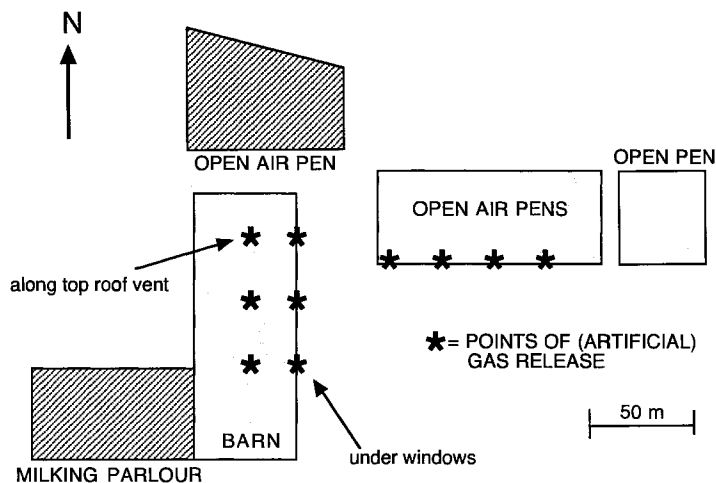


Figure 4.1: Configuration of experimental site

vents allowing air exchange. The property was bordered on its western side by a road, across which lay another farm with a crop of potatoes, and three other crop farms to the North, East and South. There were no other livestock operations for several kilometres in any direction. The fields on the property surrounding the farm buildings and pens were relatively flat and planted with tall grass, 30 – 50 cm in height.

Of the 366 cattle on the farm at the time of the experiment, 154 were lactating, and 212 were non-lactating dairy animals (this includes both dry-cows and calves).

## 4.2 Tracer Source

We used both methane ( $CH_4$ ) and sulphur-hexafluoride ( $SF_6$ ) as tracer gases. Two lines of high-density polyethylene tubing (6mm in diameter) were connected to mass flow controllers and cylinder tanks of pure  $CH_4$  and  $SF_6$  gas. Using flow hold valves, ten point sources were distributed along a ‘release line’ throughout the farm buildings and pens at locations chosen to coincide (broadly) with locations of

natural emission from the animals within the buildings and in the pens. Four of these sources were placed along the southern boundary of the east-west pens, suspended approximately 3 m above ground and out of reach of the cows; three along the side of the barn under the windows roughly 1.5 m above ground; and three along the roof of the barn next to the vent and above those positioned along the windows (see Fig. 4.1). The release line was calibrated to ensure that each of the ten  $CH_4$  and each of the ten  $SF_6$  outlets were releasing approximately the same amount of tracer gas. The calibration was performed using a standard test gas (pure  $N_2$ ) released at a known rate; a handheld flow meter was used to measure the flow rate at each of the outlets. A series of tedious adjustments ensured that, irrespective of the pressure drop along the supply tubing, there was equal output at each of the release locations. It was assumed that the calibration performed using the standard gas would yield the same balanced flow rates for the tracer gases  $CH_4$  and  $SF_6$  during the experimental release.

The tracer gases were released from high pressure cylinders; methane was released at a total flow rate of  $100 \text{ L min}^{-1}$  and  $SF_6$  at a total flow rate of  $200 \text{ mL min}^{-1}$ . Methane was released for 45 or 50 min, then turned off for 45 min repeatedly.  $SF_6$  was turned on 15 min before the  $CH_4$  and left on through both the on and off periods of methane release.

Our intention was to perform several consecutive release periods producing a sequence of stepped on-off cycles of  $CH_4$  concentrations, with periods of artificial gas release intended to be distinguishable from periods of natural emission from the farm alone. As the natural (or background) concentration of  $SF_6$  is so small that it was considered negligible, any observed concentration of  $SF_6$  was assumed to result only from the gas we were releasing. Since no other  $SF_6$  was emitted from the farm, it was not necessary to distinguish between ‘on’ and ‘off’ cycles of this tracer gas, and to

simplify procedure, the  $SF_6$  was left on through multiple periods of methane release.

## 4.3 Methane Concentration Measurements

### 4.3.1 Methane Lasers

Methane concentration was measured using a multi-path tunable diode laser and two open path methane lasers (GasFinder MC and GasFinder, Boreal Laser Inc.) In the case of the multi-channel (MC) unit, a laser beam from a tunable infrared diode is coupled with fibre optic and coaxial cables, and the signal from a single laser directed to seven different heads (Fig. (4.2)). The beam is aimed at seven distant retro reflectors (compound mirrors) where upon arrival it is reflected back to a detector at the head. Because of the matching wavelength, the beam excites molecules of the target compound, in this case methane. The amount of energy lost along the path, the energy required to agitate the methane molecules, can be quantified and is related to the average concentration of methane in the air along the beam between the laser head and the reflector. The wavelength used in the  $CH_4$  measurement by the GasFinder unit is 1653 nm; the unit is designed to scan over a minimal spectral range to prevent interference from other gas species (Desjardins et al. 2004). The stand-alone open path lasers measure methane in the same way, though the laser signal is directed only at one reflector.

The MC unit cycled through all seven channels continuously, recording a line-average concentration approximately every minute for each of the seven locations. These concentrations were then averaged into 5 minute values\*. The concentration

---

\*The data was acquired in 5 minute average values to allow us to observe the concentration ramp on and fade-out due to the artificial methane release which may have been difficult to assess using the more conventional 15 minute averaging period. These 5-min averages were later re-organized into 15-min averages, more typical of micrometeorological procedure, for input to the bLS model





Figure 4.2: One of the seven laser heads used with the multi-channel unit. The scope was used to aim the laser at the retro reflector located approximately 350 m away.

data were acquired using the GasFinder software (Boreal Laser Inc.) which stored the concentration values for each of the channels and plotted them as a function of time on screen. The GasFinder software also stored information about light levels and signal loss for each of the channels in use. The concentration data from the stand alone units was stored internally and uploaded to a computer.

### 4.3.2 Background Concentration Measurement

The natural, or atmospheric background concentration of methane was obtained by gas chromatography. Upwind samples were taken at the field site every half hour on the days when we were releasing, or expected to release the tracer gases. Three air samples were taken with a 20 mL syringe which was purged three times between samples. The vials containing the air samples were taken, daily, to a laboratory located within the Agriculture and Agri-Food research station for analysis by a technician. Although the multi-channel unit did not, according to the manufacturer, require calibration, the concentration measurements from the MC unit were never in agreement

(with respect to the error range of the instruments) with the values for background methane concentration as obtained through a laboratory analysis.

### 4.3.3 Calibration of the Gas Lasers

#### Field Calibration

To account for signal loss along the coaxial cables connecting each of the seven laser heads to the multi-channel unit, a cable compensation coefficient is applied. The cable compensation ( $cc$ ) value is applied as a multiplicative correction to the concentration output of each of the seven channels. The longer the cable from the multi-channel unit to the laser head the more signal is lost along the line, and the higher the  $cc$  value required to make up for this loss. In an attempt to compute the  $cc$  value for each of the seven channels, a pre-release field calibration was carried out.

The calibration was performed using a standard gas with 405 ppm  $CH_4$  in pure nitrogen. A three meter piece of polyvinyl chloride (PVC) tubing was fitted with a transparent window at one end and a sheet of reflective paper at the other (Fig. 4.3). At the end of the tube located nearest to the laser head was a hole into which the standard gas was pumped at a very low flow rate through a length of plastic hose connected to the tank of gas. At the opposite end of the calibration tube was an outlet through which the standard gas was slowly released.

The multi-channel unit was disabled for all channels but the one corresponding to the head at which the calibration tube was set up. The cable compensation value was set initially to 1.0 and the GasFinder software was run to record the concentration values of  $CH_4$  inside the 3 m calibration tube. The concentration recorded by the laser was allowed to stabilise before the  $cc$  value was stepped up to 1.1, 1.3 and

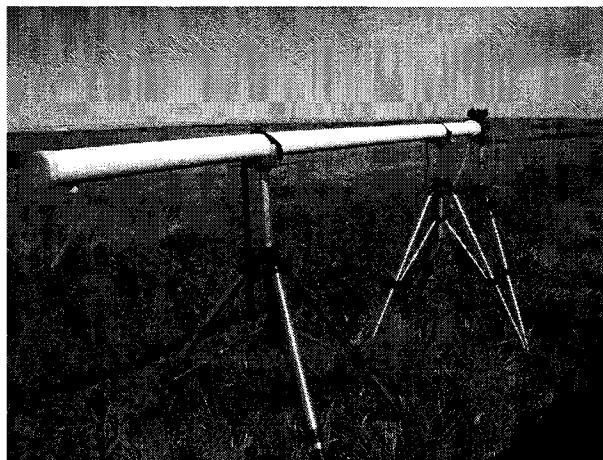


Figure 4.3: This 3 m tube was used with a standard test gas in the field calibration.

1.5<sup>†</sup>, values chosen to give concentration data for  $cc$  values in the MC unit's range of 1.0 – 2.0.

The average concentration reported by the instrument under calibration for each of the four  $cc$  values was then plotted against the compensation value. As the  $cc$  value acts as a straight multiplier on the concentration reported by the channel, the relationship is linear. An example of the plot used to generate the cable compensation for Channel 4 is shown in Fig.(4.4)<sup>‡</sup>. The results of the field calibration are given in Table (4.1).

### Retrospective Calibration

Unfortunately the field calibration that was carried out proved unsuccessful. The 'corrected' concentration values were unrealistic for all but one of the seven channels. After spending three potential release days performing calibrations, it became obvious

---

<sup>†</sup>As a standard gas was used, with a known concentration of  $CH_4$ , over a fixed and known path length it could be seen qualitatively what value of  $cc$  was needed to bring the concentration as recorded by each channel to the appropriate level.

<sup>‡</sup>The unit ppmm refers to 'parts per million meters' and is used when dealing with line concentration sensors giving the line integral of the local concentration (ppm) along the path of the laser.

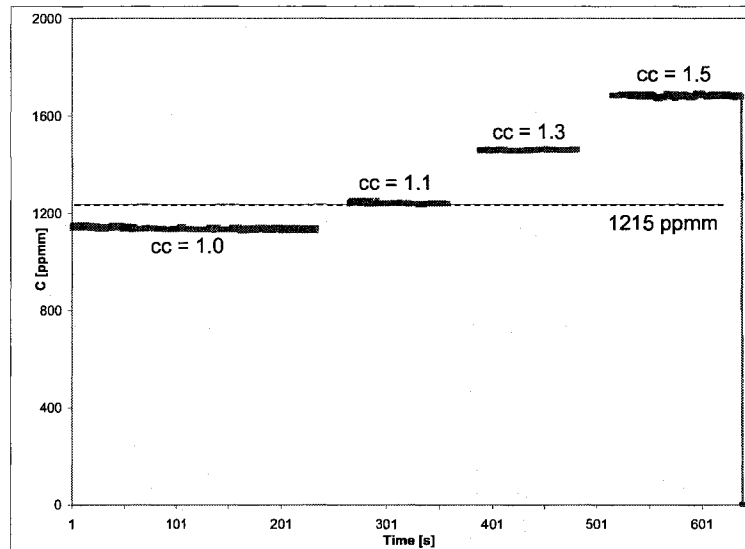


Figure 4.4: Example of plot used to obtain a cable compensation value with the field calibration. The y-axis is the reported ppmm value of the test gas (405 ppm  $CH_4$  with a 3 m tube), the dashed line indicates the true value of 1215 ppmm. The  $cc$  value obtained from this calibration was  $cc = 1.09$ . It can be seen qualitatively that the value closest to the true concentration is obtained using a  $cc$  value of 1.1.

that it would be necessary to resort to a retrospective calibration that was carried out after the completion of the field experiment.

Background methane concentration was known from the gas chromatography analyses performed on samples of air taken at the site upwind of the farm complex. Five minute averages of wind direction and concentration were available for each of the seven sensors for the period between the 30th of September and the 5th of October. For each of the seven sensors, the complete data set was filtered with respect to wind direction to leave only those periods during which the given sensor should be reading only a background concentration of methane (ie. periods when that particular sensor was located upwind from the farm). A calibration factor forcing the average concentration for that sensor over that period to the known value of background concentration was applied. This process was repeated for each of the seven sensors of the multi-channel unit and for the two stand alone units as well.

Head	Field	R1	R2	R3	R4
1	1.16	1.01	0.99	1.27	1.23
3	1.10	0.99	1.01	1.12	1.04
4	1.03	1.11	1.26	1.27	-
5	1.33	0.97	1.08	-	-
6	1.17	0.89	-	-	-
7	1.56	1.17	1.10	-	-
8	1.12	0.83	0.76	0.89	-
NSA	-	0.91	-	-	-

Table 4.1: Cable compensation values resulting from both the field and retrospective (R1-R4) calibrations, for all seven laser heads

Most disconcertingly, the results of this retrospective calibration yielded compensation values that varied from day to day for the same sensor. In several cases there were multiple periods when a particular head was located upwind of the farm. When these periods were used in the calibration to give a (mean) concentration that matched the value obtained from the GC analysis, they produced a range of results. The heads were calibrated using the compensation value calculated for each day where data was available. In cases where a compensation value for a particular day was not available, the value for the previous day was used for that head. The compensation values resulting from the retrospective calibration ( $R1 - R4$ ) are given along with the corresponding values from the field calibration in Table (4.1).

#### 4.3.4 Laser Positions

The farm buildings, pens and the animals contained therein were treated as a uniform area source. This assumption is considered an acceptable first approximation as the sensors used to measure methane concentration emitted from the animals were deemed to be sufficiently far away as to render the distinction between many point sources and an equivalent, effectively- uniform area source negligible. Van Ouwerkerk

(1993) has shown that for measurements beyond a distance of ten farm heights, where the farm height is taken as the height of the tallest building (in our case approximately 8 m), a farm may be considered a uniform area source. The distance from the farm

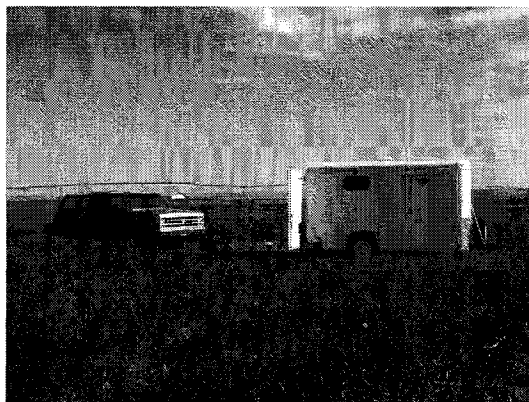


Figure 4.5: The trailer housed the multi-channel unit, and the laptop computer.

that we were able to achieve was limited only by the multi-channel laser unit's need for AC power and the distance we were able to cover with several extension cords to the closest outlet. The multi-channel unit was operated from inside a trailer (see Fig. 4.5). The seven heads were connected to the multi-channel laser through a coupled fibre-optic and coaxial cable. The fibre-optic cables were quite sensitive to bends or kinks in the lines, and would fail to deliver enough light to the head if they were not laid out reasonably straight and flat along the ground. We had access to six 50 m cables and two 150 m cables, which dictated the laser head locations around the trailer housing the multi-channel unit. Unfortunately one of the two 150 m cables failed to deliver enough light to the head and it was replaced with a stand-alone unit in the same position.

The lasers were placed at distances from 50 – 250 m from the farm complex. The distance from the farm to the laser is given as the nominal distance from the closest

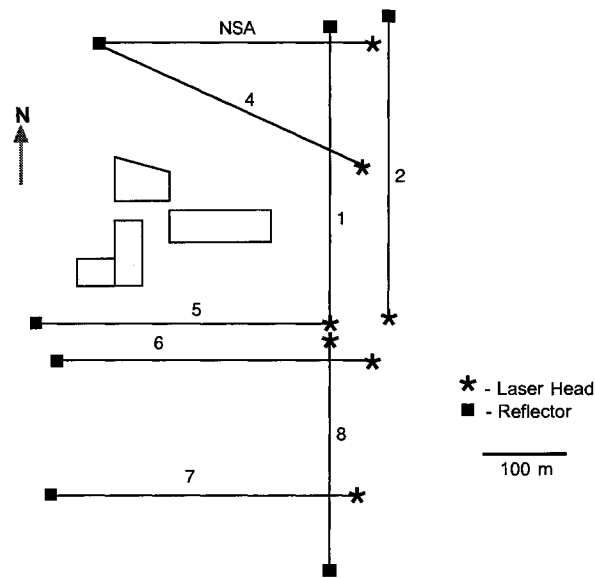


Figure 4.6: Locations of laser heads around the farm. The numbers 1-7 refer to the channels that were used with those laser heads, the laser labelled ‘NSA’ (North Stand-Alone) refers to the stand-alone unit used at the northernmost location.

farm boundary parallel to a particular laser path. For example, Laser 1 in Fig. (4.6) ran north-south. The distance from the farm to Laser 1 is given as the distance between the easternmost north-south wall of the pens to the path of Laser 1. It should be stressed here that these distances, or fetches, are nominal, and used only to give the reader the sense that the lasers were placed at varying distances from the farm complex.

Our initial intention was to be consistent in path length for all seven lasers, but limited accuracy with the GPS and property boundary restrictions made this impossible. The path lengths therefore ranged from 278 – 368 m. A GPS unit was used to aid in the establishment of landmarks which allowed us to position the laser heads and reflectors along approximate east-west and north-south lines. For consistency, all

Head	Fetch	Path
1	50	368
3	170	348
4	150	326
5	95	350
6	147	348
7	250	349
8	300	278
NSA	200	318

Table 4.2: The fetch (nominal distances from the farm to the sensor) and path length for each of the laser heads, given in meters.

laser heads were set at a height of 1.4 m and all reflectors at a height of 1.5 m<sup>§</sup>. The configurations of the laser paths around the property are shown in Fig. (4.6). A list of path lengths and distances from the farm complex is given in Table (4.2).

The configuration of the lasers around the farm complex was most advantageous for winds from the North, winds from the West, or any direction in between.

#### 4.4 $SF_6$ Measurements and the Sample Line

The concentration of the tracer gas  $SF_6$  was obtained through gas chromatography analyses of air samples taken during the tracer release. A ‘sample line’, a 200 m length of polyethylene tubing (6 mm in diameter) was fitted with ten intake valves evenly spaced along the line. A 12V D.C., battery operated pump (TD3LS7; Brailsford and Company) drew air into the line through the 10 intake valves. The flow rate through each intake was adjusted to be equal and was approximately 2 L min<sup>-1</sup>. Every five minutes during a period of  $SF_6$  release, a sample of air was taken from the line using a

---

<sup>§</sup>The software used to implement the bLS model allows the user to specify both the ‘start’ and ‘end’ height (laser head and reflector) of the line concentration sensor. The (slight) angle of the beam due to the height difference between the laser and the reflector is accounted for in the model software.



syringe and a septum port. The content of the syringe was immediately emptied into an evacuated vial (6.8 mL volume) through a double septum cap. The time and date were recorded on the vial. These samples were then analysed by gas chromatography to obtain values of  $SF_6$  and  $CH_4$  concentration at the location of the sample line during the release period. An open path laser (Boreal Laser Inc.) and retro-reflector

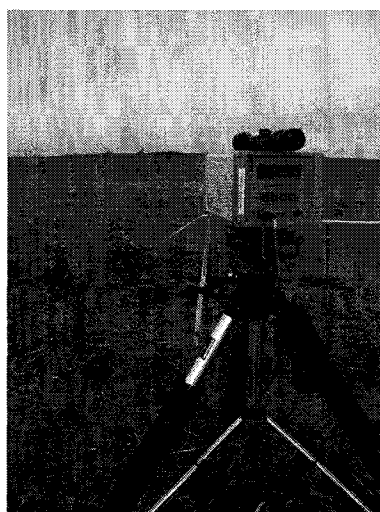


Figure 4.7: An open-path laser was run parallel to the sample line, and was used to check the calibration of the laser against the values of concentration obtained through GC analysis.

were placed parallel to the sample line and along approximately the same path during the release periods (Fig. 4.7). The values of  $CH_4$  concentration obtained from the GC analysis were used to calibrate that particular laser.

## 4.5 Meteorological Observations

A 5-m mast mounted on a flatbed trailer supported a 3D sonic anemometer (CSAT-3, Campbell Scientific) mounted 3-m above ground, and a wind vane at the top of the mast (see Fig. (4.8)). Data acquisition was performed by a Campbell Sci-

entific (CR23X) data logger, computing averages over 5-minute periods, positioned on the trailer and with its battery charged by two solar panels.

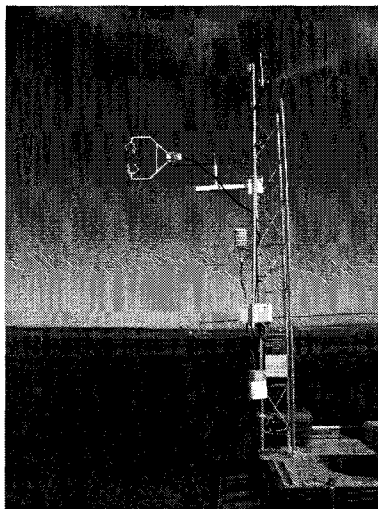


Figure 4.8: Meteorological measurements were made with a 3-D sonic anemometer which was mounted on the tower shown here.

The orientation of the frames of the sonic anemometer and the wind vane were determined using a global positioning system (GPS) with respect to a north-south co-ordinate system:

$$\beta = \tan^{-1} \left( -\frac{V_{raw}}{U_{raw}} \right) + \beta_{offset}, \quad (4.1)$$

where  $V_{raw}$  and  $U_{raw}$  are the average horizontal velocities with respect to the frame of the sonic, and  $\beta_{offset}$  is the angular offset of the sonic with respect to our co-ordinate system. Raw heat flux and velocity statistics were transformed (using two coordinate rotations) into along wind coordinates (Kaimal & Finnigan 1994). Using these transformed velocities we calculated the friction velocity, the Obuhkov length

and the roughness length,

$$u_* = (\overline{u'w'^2} + \overline{v'w'^2})^{1/4}, \quad (4.2)$$

$$L = -\frac{u_*^3 T}{k_v g \overline{w'T'}}, \quad (4.3)$$

$$z_0 = \frac{z_{sonic}}{\exp(\overline{u}k_v/u_* - \psi)}, \quad (4.4)$$

where  $\overline{u'w'}$  and  $\overline{v'w'}$  are velocity fluctuation covariances,  $T$  [K] is the (acoustic) air temperature given by the sonic anemometer,  $g$  the gravitational constant,  $k_v = 0.4$  is von Karman's constant,  $\overline{w'T'}$  is the vertical heat flux, and  $\psi$  is a stability correction (see Flesch et al. 2004).

## Chapter 5

### Data Analysis and Results: Dairy Farm Emissions

#### 5.1 Data Filtering

Not all observational periods were used to compute emission estimates. Our observation periods were five minutes in duration. These five minute periods were reorganized into 15 minute averages for input to the bLS model. Many of these periods were not included in the emission estimates because of a misalignment of the laser head with the reflector, or because of an insufficient amount of light being delivered by the multichannel unit to the laser head\*. Periods of high wind were also unsuitable for sampling as the lasers were quite easily blown out of alignment with their reflector targets resulting in a loss of signal. During several other observational periods the wind direction was not compatible with our set-up and the farm plume was not blown through any of the laser paths, making an emission inference impossible.

Following Flesch et al. (2005) observational periods when the Monin-Obuhkov length  $|L| \leq 2$  (i.e. periods when the atmospheric surface layer was unlikely to be well described by the Monin-Obuhkov Similarity Theory) were removed. Flesch et al. (2005) found that periods of extreme stability lead to inaccurate emissions estimates

---

\*The system was quite sensitive to changes in temperature and would not work at all when it was cold ( $T \leq 2$  C). This made early morning sampling, though ideal in terms of the wind, impossible.

using the bLS model. It was also found that values of  $u_* < 0.15\text{ms}^{-1}$  correlate with inaccurate predictions of  $Q_{bls}$  and such low-wind periods were removed.

In some observational periods the farm plume only barely passed through the path of the sensor. The software used to run the bLS model allows the user to record the fraction of the source area that was covered by particle touchdowns during the model run, and periods in which less than  $2/3$  of the source was covered were excluded from emission estimates. Fig. (5.1) gives an example of good and bad coverage of the area source by model particles. As a result of this filtering several periods of data were excluded and the results presented here are for three release periods on September 30th and October 2nd, 2005.

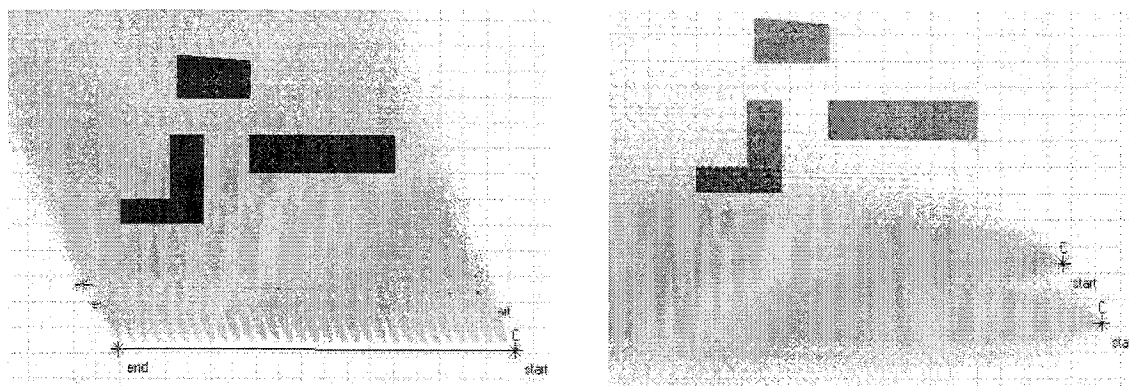


Figure 5.1: The figure on the left depicts an example of good source area coverage, while the figure on the right depicts an example of bad source area coverage which would not be included in the emission estimate. The light grey area represents the ‘plume’ of computational particles. Interaction of these particles with the source area results in a dark grey colour on the source. In the image on the left, the source is almost entirely covered in particles, while in the figure on the right most of the source area has not had any interaction with the plume of computational particles. The WindTrax software displays the sensing laser as a line joining “start” and “end”.

## 5.2 Emission Estimates

### 5.2.1 Backward Lagrangian Stochastic Model

In this experiment a line-average concentration is measured by each of the seven laser heads of the multi-channel unit, as well as by the two stand-alone open-path lasers. Any one measurement of concentration  $C_L$  is a possible basis for the inference of an emission rate  $Q$ .  $C_L$  (as seen by any one laser) is modelled as the average of  $P$  point concentrations which are located evenly along the laser path (Flesch et al. 2004). From each of these points an ensemble of (backward) trajectories is computed, and,

$$(C_L/Q)_{mod} = \frac{1}{P} \sum_{j=1}^P \left( \frac{1}{N_p} \sum \left| \frac{2}{w_0} \right| \right), \quad (5.1)$$

where  $N_p$  is the number of particles released from each point and the second summation is only for touchdowns within the source area. The emission rate  $Q_{bls}$  is computed by

$$Q_{bls} = \frac{(C_L - C_b)}{(C_L/Q)_{mod}}, \quad (5.2)$$

where  $C_b$  is the atmospheric background methane concentration, and the subscript ‘mod’ refers to the model computation. The measured background methane concentration was 2.03 ppm on September 30th and 2.00 ppm on October 2nd.

### 5.2.2 Application of the bLS Model

The bLS model is implemented using WindTrax (Thunderbeach Scientific) software. The Obuhkov length, the friction velocity and the roughness length,  $(L, u_*, z_0)$ , as computed for the averaging interval (15 minutes) are used as inputs. In each simulation  $N_p = 50,000$  particles were released from each sensor location  $(x_s, y_s, z_s)$ . The particles are released with random velocity consistent with properties of the wind

at location  $z_s$ , the height of the sensor, in our case  $z_s = 1.4$  m. To represent a line average concentration when calculating  $(C_L/Q)_{mod}$ ,  $P = 50$  points along the sensor were used. The horizontal position and vertical velocity at each particle touchdown are recorded.

As we had concentration data for up to 9 laser heads as well as very accurate background concentration data from the GC analysis, the bLS software was run using various sensor configurations to obtain multiple emission estimates for each of the three release periods. WindTrax allows the user to place as many sensors as is desired around the (uniform) area source. The height of both the laser head and the reflector are specified along with the species of gas measured by the sensor (in our case  $CH_4$ ). Regardless of how many sensors are used, each is treated independently in the emission computation, the final estimate being a result of a least squares computation<sup>†</sup>.

Because of a discrepancy between (observed) concentration data from different laser positions<sup>‡</sup>, the bLS model was run using several configurations of the sensors to make an emission estimate. Details of all configurations used are given in Appendix 2.

### 5.2.3 Ratiometric Computation

Once the concentration of  $SF_6$  had been determined (by GC analysis), the source strength of methane being emitted from the farm could be obtained by means of a ratiometric computation. Recall that an artificial source of methane, co-located with the source of  $SF_6$  is being switched on and off at roughly 45 or 50 min intervals during release. The total concentration of methane due to emissions from the farm and the

---

<sup>†</sup>the value of  $Q$  which minimizes  $\sum_i^n d_i^2 = \sum_i^n (C_i - C_{(mod)i})^2$  where  $C_{mod}$  is the model estimate (or fitting curve) and has the deviation (error)  $d_i$  from each value  $C_i$  (from each sensor), ie.  $d_1 = C_1 - C_{(mod)1}, \dots, d_n = C_n - C_{(mod)n}$

<sup>‡</sup>Even after calibration, L5 gave lower concentration values in some observational periods than L6 which was located roughly 50 m further downwind from the source. There were additional examples of this discrepancy with other pairs of parallel laser heads of the multi-channel unit.

release of artificial methane,  $C_{CH_4}(total)$ , may be estimated by taking the concentration given by the laser during a release period, and subtracting the atmospheric background methane concentration. The ratio of the total methane concentration,  $C_{CH_4}(total)$ , to the concentration of sulphur-hexafluoride,  $C_{SF_6}$  must, by assumption, be equal to the ratio of the source strength of methane,  $Q_{CH_4}(total)$ , to the source strength of  $SF_6$ , as in Equation (5.3):

$$\frac{C_{CH_4}(total) - C_b}{C_{SF_6}} = \frac{Q_{CH_4}(total)}{Q_{SF_6}}. \quad (5.3)$$

The experiment permits one to deduce the only unknown,  $Q_{CH_4}(total)$ , from Eq. (5.3). Then, since the source strength of the added methane,  $Q_{CH_4}(artificial)$  is known, the amount of methane emitted by the farm alone, is:

$$Q_{CH_4}(farm) = Q_{CH_4}(total) - Q_{CH_4}(artificial). \quad (5.4)$$

The ratiometric method gives us a ‘model free’ estimate of emission from the farm. This method does not rely on any knowledge or modelling of atmospheric processes or parameters, and the concentration data obtained through GC analysis is very accurate. Results from the ratiometric computation provide us with an emission estimate with which to compare the bLS results, and give us a method of testing the efficacy of the bLS technique.

While the ratiometric method is model free, we are assuming that the air samples taken from the sample line are well mixed and may be interpreted as line average concentrations. Likely sources of error in the ratiometric computation include: measurement error associated with the GC analysis (these are quite small, of the order of 0.001 ppm for  $CH_4$  and 10 ppt for  $SF_6$ ); variation of the flow rate of both the artificial  $CH_4$  and the  $SF_6$  release ( $\pm 20$  L min<sup>-1</sup> in the case of  $CH_4$  and  $\pm 10$  mL min<sup>-1</sup> in the case of  $SF_6$ ); and error associated with flow rates given by the mass flow con-



trollers (roughly  $\pm 10 \text{ L min}^{-1}$  for  $\text{CH}_4$  and  $\pm 5 \text{ mL min}^{-1}$  for  $\text{SF}_6$ ). Finally, and perhaps most importantly, please note that since the source distribution of the added methane only approximates the natural source distribution of methane, the estimate for  $Q_{\text{CH}_4}(\text{farm})$  provided by Equations (5.3 and 5.4) and the ratiometric method is itself only *approximate*.

## 5.3 Results

### 5.3.1 bLS Estimate of ‘Whole-Farm’ Emissions

The concentration time series, as recorded by the GasFinder software during the field experiment, are shown for the 30th of September and the 2nd of October in Fig.

(5.2) and Fig. (5.3) respectively.

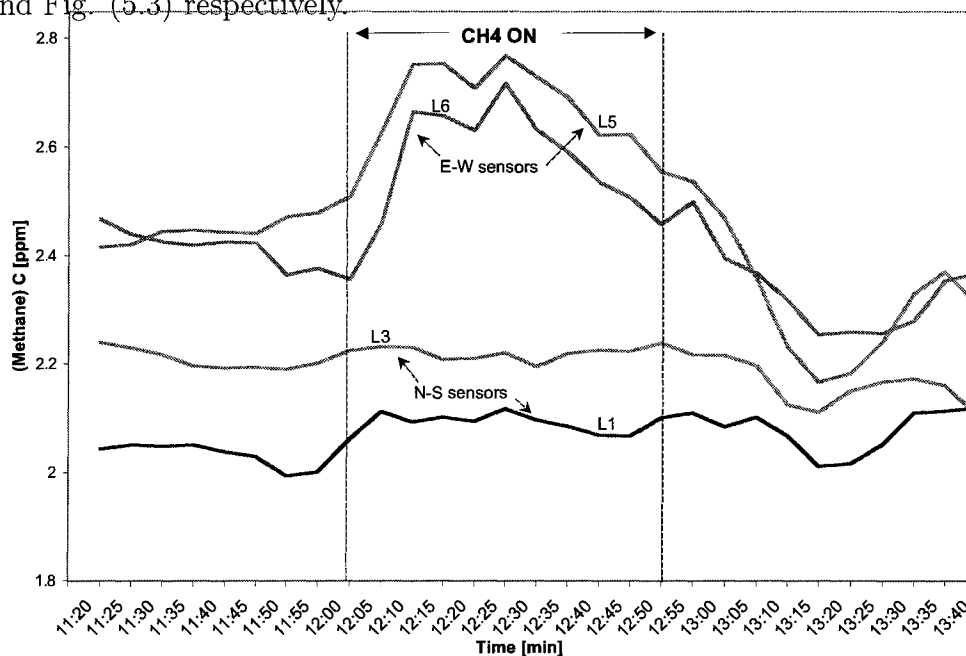


Figure 5.2: The concentration time series recorded during the field experiment on Sept. 30th. The artificial methane release began at 12:00 and ended at 12:50.

The corresponding emission time series for the September 30th release is shown

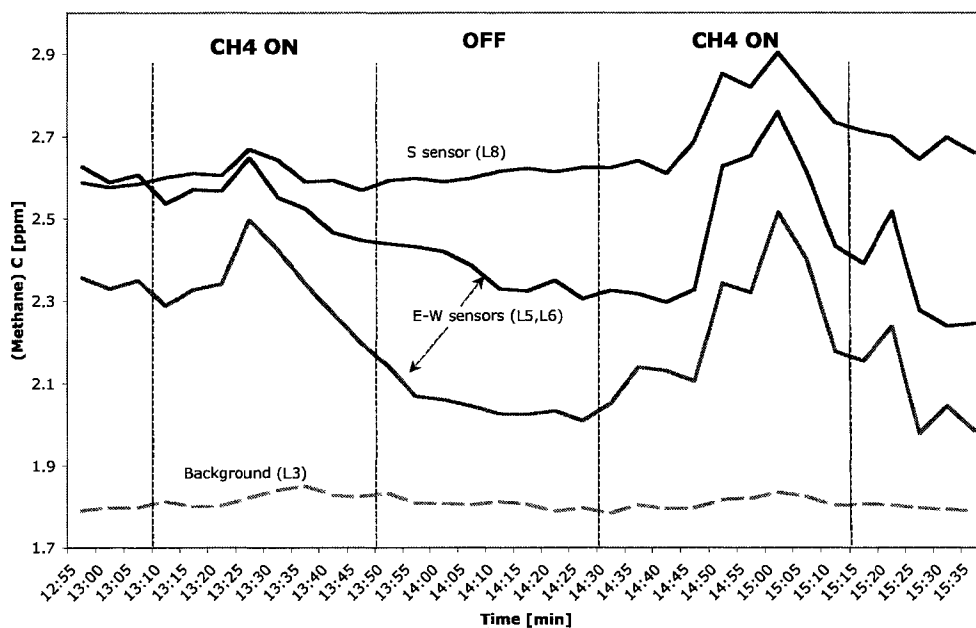


Figure 5.3: The concentration time series recorded during the field experiment on Oct. 2nd. The first artificial methane release period began at 13:10 and ended at 13:50, and the second release period began again at 14:30 and ended at 15:15.

in Fig. (5.4). The expected relationship between concentration and emission can be seen qualitatively from the shapes of the curves in Fig. (5.2) and Fig.(5.4). The emission is seen to ramp up during the period of artificial gas release and follows the same shape as the concentration time series. The dashed-line curve ‘C(L5)’ in the plot shown in Fig. (5.4) is the concentration data from Laser 5 (the closest E-W sensor to the farm (see Fig. 4.6) given in ppm. The dotted and solid lines ‘Q1’ and ‘Q2’ are the emission estimates resulting from two different input configurations in WindTrax given in  $\text{g s}^{-1}$ . The square wave represents the magnitude of the artificial methane release,  $1.19 \text{ g s}^{-1}$ , which was released from 12:00 to 12:50.

The emission values obtained using the bLS model and WindTrax as well as those obtained through the ratiometric computation are given in Table (5.1). All values are given in  $\text{g day}^{-1}$ . The ‘Gas On’ entries refer to periods of artificial methane release.

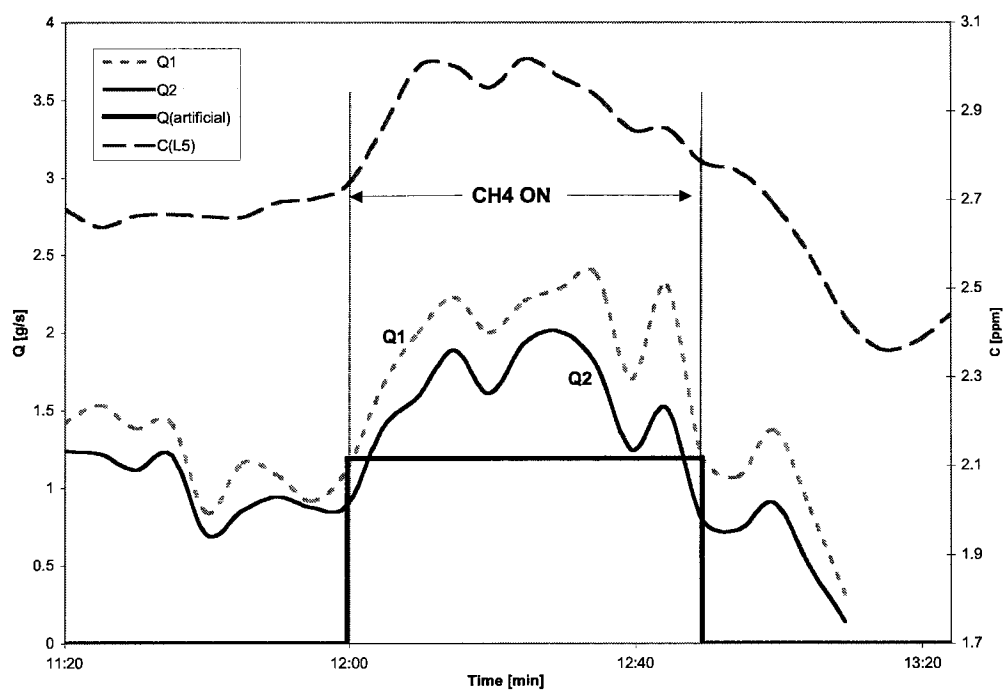


Figure 5.4: The emission time series resulting from the bLS model computation, using the concentration data from the Sept. 30th release period (gas on from 12:00 to 12:50). On the second y-axis is concentration in ppm. The square wave indicates the source strength of the added methane.

The amount of methane added, ( $1.19 \text{ g s}^{-1}$ ), along with the contribution from the background concentration have been subtracted to give a ‘farm only’ value. The ‘Gas On’ emission estimate is the average over the middle 15 min of the release period to avoid including those periods when the artificial gas ramps on and fades-off. The ‘Gas Off’ entries were obtained by averaging the 15 minutes leading up to a release and the 15 minutes immediately following the end of the release.

There was good consistency between the emission estimates made during a period of artificial methane release and those periods before and after a release. However, the results of the ratiometric computation are inconsistent with estimates made using the bLS model. As the concentrations obtained by GC analysis were used in the ratiometric method, and these concentrations are considered more accurate than those obtained with the lasers, this discrepancy was a cause for concern.

Release Date	Gas On	Gas Off	Ratiometric
Sept30	82626	85418	43200
	73948	68504	
	80154	72415	
Oct2	74742	73489	36288
	87200	88905	31968

Table 5.1: Farm (only) emission estimates for the Sept. 30th and Oct. 2nd releases. The second column (‘Gas On’) refers to an emission estimate made by subtracting the artificial methane from the total emission over the release period, the ‘Gas Off’ value is an estimate of emission made when no artificial gas was released. All values are given in  $\text{g day}^{-1}$ . Note that the “ratiometric” estimate is based on GC sampling from an intake line, whereas the other two columns hinge on the application of the bLS to those laser detectors standing in the plume off the farm.

In an attempt to determine the root of the disagreement between the the two sets of results, the bLS model was run using the location of the sample line and the concentration data from the GC analysis as a ‘sensor’ input. In WindTrax, a

line-average concentration sensor<sup>§</sup> was placed in the position and orientation that the sample line had been in, using the GPS coordinates taken at the experimental site for both the September 30th and October 2nd release days. The 5-min (line-average) concentration values taken by syringe and GC analysis during the release period were used as concentration inputs to the model<sup>¶</sup>.

Release Date	WindTrax	Ratiometric
Sept30	35424	43200
Oct2	32832	36288
	31104	31968

Table 5.2: Farm (only) emission estimates based on the sample line data, comparing the bLS and the ratiometric estimates. All values are given in  $\text{g day}^{-1}$ .

The resulting bLS estimates are compared with the ratiometric estimates in Table 5.2. As expected, the bLS model emission estimate using the sample line data is reasonably consistent with the ratiometric computation, and about 50% lower than those bLS emission estimates which were made with the concentration data *from the lasers*.

However, it became clear after a visual assessment of the touchdown catalogue for the model run using the sample line data that *the sample line was only picking up part of the plume released from the farm*. Most importantly it could be seen that the sample line was only seeing a contribution from four of the ten point sources of artificial release. Two 5-min periods of the bLS model run using the GC data from the sample line location are shown in Fig. (5.5). Recall that six of ten point sources

<sup>§</sup>measuring  $CH_4$ , and of length 200 m - the same as the sample line

<sup>¶</sup>Although the Monin-Obuhkov wind statistics used in the WindTrax software are based on experiments which used longer averaging times (15-60 min.) when the GC data was input to the bLS model, the 5-min average values were retained. Not all the air samples taken during the release were good - some bad vials with broken seals were identified - and some of the 5-min periods were missing from the analysis altogether. It was therefore deemed preferable to run the model using the 5-min average values then to attempt to re-average into 15 min values.

are located along the windows and roof of the barn. It is obvious from Fig. (5.5), that the sample line only saw a contribution from those point sources located along the row of pens, and not from those located on the barn. This would have resulted in much lower concentrations of both  $CH_4$  and  $SF_6$  at the sample line, biasing estimates of the true rate of emission so as to be lower than expected.

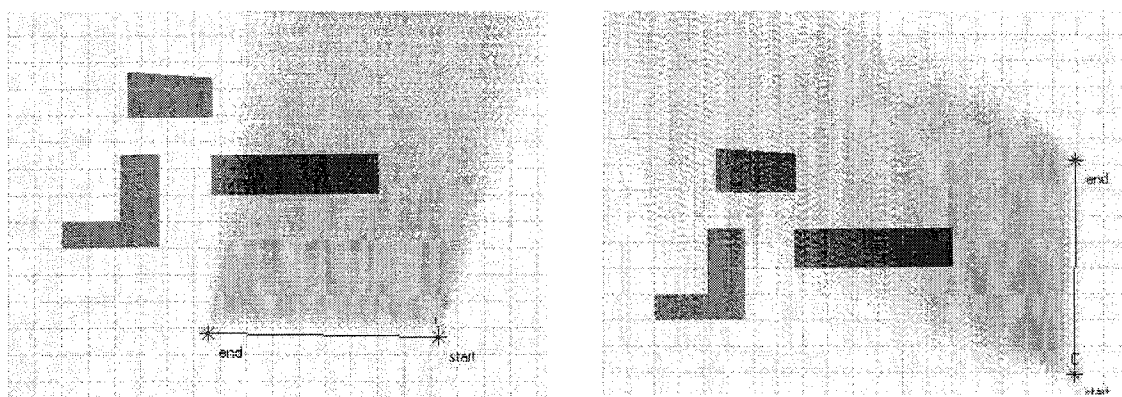


Figure 5.5: Examples of (5-min) period of the bLS model run using the GC data and the sample line location as inputs. On the left is the configuration of the sample line for September 30th, and on the right the configuration for October 2nd.

The ratiometric estimates were corrected by scaling  $Q_{SF_6}$  and  $C_{CH_4}(total)$  by a factor of  $10/4$  to compensate for the contribution from 6 out of 10 point sources not seen by the sample line during the release. The corrected values of emission using the ratiometric computation as well as the estimates made using the bLS model are shown in Table 5.3. The emission values are given in  $g \text{ animal}^{-1} \text{ day}^{-1}$  and the three estimates for the 30th of September and the two estimates for the 2nd of October have been averaged together. Kinsman et al. (1995) found that a lactating animal emits  $400 \pm 42 g \text{ animal}^{-1} \text{ day}^{-1}$  and Marik and Levin (1996) have shown that a non-lactating (dairy) animal emits roughly half that amount. Applying these values to the ratio of lactating to dry animals at the farm at the time of the experiment,

Release Date	Gas On	Gas Off	RM	RM'
Sept30	216	206	118	295
Oct2	221	222	94	213

Table 5.3: Emission estimates for the Sept. 30th and Oct. 2nd releases. All values are given in  $\text{g day}^{-1} \text{ animal}^{-1}$  and the bLS estimates are within  $\pm 35 \text{ g day}^{-1} \text{ animal}^{-1}$ . The RM' column gives the corrected ratiometric results. (Note: except for column RM', values differ from those of Table 5.1 only due to the different units.)

( $\frac{154}{366}$  lactating and  $\frac{212}{366}$  dry cows and calves), gives  $284 \text{ g animal}^{-1} \text{ day}^{-1}$ , an estimate that is reasonably consistent with the emission estimates obtained here, bearing in mind the many factors which can cause a variation in this rate.

### 5.3.2 bLS Estimate of Artificial Source Strength

The WindTrax estimate for the source strength of the artificial methane was deduced from a comparison of the emission estimates made during a period of artificial release and those made when no artificial methane was released. The  $CH_4$  source strength estimates are compared to the value given by the flow meter in Table 5.4. The 'Gas On' entries are emission estimates for contributions from the farm and the artificial methane. The 'Gas Off' entries are, as before, the average of the 15 minutes leading up to release, and the 15 minutes immediately following the end of the release. The 'Difference' entries are the 'Gas On' estimates minus the 'Gas Off' estimates, and are the bLS prediction of the source strength of the artificial methane.

The bLS estimates of the source strength of artificial methane 'Q(bLS)' for September 30th, for October 2nd and the average of these values are given in Table 5.5 along with the source strength from the flow meter 'Q(flow meter)'. It can be seen from Tables 5.4 and 5.5 that the (average) bLS estimate of the source strength of the artificial methane ( $1.21 \text{ g s}^{-1}$ ) agrees well with the value given by the flow meter ( $1.19 \text{ g s}^{-1}$ ).

Release Date	Gas On	Gas Off	Difference	Q(flow meter)
Sept30	185442	85418	100024	102902
	176764	68504	108260	
	182970	72415	110555	
Oct2	17758	73489	104069	102902
	190016	88905	101111	

Table 5.4: Emission estimates for the Sept. 30th and Oct. 2nd releases used to deduce the bLS estimate of the source strength of the artificial methane. All values are given in  $\text{g day}^{-1}$ .

Release Date	Q(bLS)	Q(flow meter)
Sept30	1.16	1.19
	1.25	
	1.28	
Oct2	1.17	1.19
	1.20	
Average	1.21	1.19

Table 5.5: bLS estimates for source strength of artificial methane and the average value of these. All values are given in  $\text{g s}^{-1}$ .



## Chapter 6

### Conclusions

This experiment has shown that the bLS model technique can diagnose the ‘whole-farm’  $CH_4$  emission rate of a commercial dairy farm. Emission estimates made by means of a ratiometric computation using the tracer gas  $SF_6$  confirm the good performance of the bLS model in this situation.

It was assumed that the whole farm\* could be treated as a uniformly-releasing area source provided our concentration sensors were located sufficiently far away as to render the distinction between many individual point and area sources and one uniform area source negligible. It was also assumed that the emitted plume was undisturbed by interaction with buildings, fences, and other obstacles. Despite these assumptions, the realistic estimates for methane emission from the farm suggest that the bLS technique is valid under these circumstances.

Several sources of error exist in the bLS estimate and the ratiometric estimate against which it was compared. It is believed that the most significant source of this error stems from instrumentation, and in particular from the multi-channel laser unit used to measure  $CH_4$  concentrations. Calibration of the (seven) laser heads of the multi-channel unit was a labourious task. A straight multiplier was expected for

---

\*including the buildings, pens, animals, and animal waste

each individual head to account for signal loss along the co-axial cable connecting the head to the laser. It was found however, during a retrospective calibration, that the compensation factor for each head varied from day to day in an unpredictable manner<sup>†</sup>. Observed line-average concentrations are used in the bLS model to infer the emission rate, and flawed concentration data will certainly result in erroneous emission estimates.

While the bLS technique is, in my opinion, a viable method to estimate emissions on the farm scale, it might be advisable to use concentration sensors that require less set-up and calibration. The cables connecting the multi-channel unit to the laser heads were very heavy and difficult to move. The fibre optic cables were very fragile, and two (of seven) had to be replaced during the course of the 6 week long field campaign. Unlike the coaxial cables, which are protected by a thick, robust, plastic coating, the fibre optic cables were coated with a thin plastic that was easily torn. Set-up of this system at the commercial farm required that the cables were laid out in large stretches of tall grass in the fields surrounding the farm complex, and one of the fibre optic cables was chewed through (on several locations) by some of the mice who made a home in our equipment trailer.

One of the expected advantages of using the multi-channel system was the number of laser heads, and locations around the farm that these would enable us to use. Because of the wind direction encountered on the release days, in the analysis, only concentration data from two (parallel) sensors running E-W, and two (parallel) sensors running N-S were used. Tedious set-up along with retrospective calibration of the MC unit lead me to suggest that using stand-alone open-path laser sensors at

---

<sup>†</sup>The variation in calibration was not found to be correlated with changes in temperature which was one of the hypotheses put forth as we started with relatively warm temperatures that dropped as the experiment was carried out.

a two (or three) locations around the farm would have yielded similar results with much less labour in this experiment.

While the emission estimates made using both the bLS model and the ratiometric technique are in fairly good agreement with the 400g animal<sup>-1</sup> day<sup>-1</sup> estimate of Kinsman et al. (1995) for Canadian dairy cows, also by means of an infrared gas analyser and a bLS model, it is clear that the two results are different. Experimental error may account for the bulk of this discrepancy, but other factors should also be considered. Seasonal variability in the amount of methane emitted by the animals, the feed given to the cattle, milking practices, and the farm location are possible explanations for the difference between the results of Kinsman et al. (1995) and those obtained here.

It has been shown using the ERUCT technique that significant variability exists in the amount of methane emission from one animal to another. The application of the bLS technique to a whole farm situation has shown that there is also variability in the per animal estimates resulting from different techniques. This suggests that the same caution used when scaling up from one animal to whole herds with results from the ERUCT technique should be exercised when using the per animal (per day) estimates obtained with the bLS model here, to other commercial dairy farm situations.

Most micro-meteorological measurement techniques are unable to detect small changes in emission estimates. Based on the present work, that limitation likely applies to bLS as well: ie. the assertion that the bLS technique might be used as a tool to measure changes (with any luck, reductions) of emission from agricultural sources in the context of the Kyoto protocol and other emission reductions strategies is questionable, unless those changes are very large (50% or greater). It is more realistic that the impacts of diet manipulation and feeding strategies on domestic ruminants

on a per animal basis should be evaluated by other means. However, it has been shown here that the bLS technique provides us with a method of estimating emission from whole farms with some confidence. This method is suitable for application to real agricultural settings and is a valid approach to the estimation of emissions from complex sources.

# Appendix 1

## Forward Lagrangian Stochastic Model Code

```
c-----
c program: Trans.f          Author: E.Shadwick      last revised: 17JAN06
c
c function: Forward Lagrangian Model for a transient source in the ASL
c
c compile with: ifort -o OnOff.exe Trans.f        Np = 1.0E+05, dt = 5
c   run with: ./OnOff.exe
c-----
      implicit none
c Reals =====
      real Ustar             ! Frictional velocity (m/s)
      real Sc               ! Schmidt number (0.63)
      real kv               ! von Karman
      real Zo               ! Surface roughness length
      real Co               ! "universal" constant
      real Xp,Yp,Zp,Wp,Up,Vp ! position/velocity
      real Ubar, Vbar       ! mean U and V (mean wind)
      real Xprev
      real dZ,dX,dY,dW,dU,dV ! position/velocity increments
      real deltaX           ! "depth" of laser
      real deltaY           ! size of bin
      real deltaZ           ! size of bin

      real Xlsr,Zlsr        ! laser postions
      real hs               ! source height
      real Zrflt            ! particle reflection height

      real Tl_u, Tl_v, Tl_w ! Lagrangian time scale
      real dtu, dtv, dtw   ! time increments
      real tsrc, dtrez     ! source and residence time
```

```

real trez(500,-1:64)           ! residence time
real tbar(500,-1:64)          ! mean residence time
real time(12)
real dt, deltat,t             ! time step

real b, e                      ! U, V, and W coefficients
real au, av, aw
real sigmaU, sigmaV, sigmaW   ! velocity variances

real dxi_u, dxi_v, dxi_w      ! gaussian random numbers
real ru, rv, rw               ! gaussian random numbers
real Q                         ! source strength [kg/m^3]
real C(500,-1:64)             ! array for concentrations
real meanC(-1:64)            ! array for mean concentration
real avg                       ! 5 minute average value
real ran3, gasdev             ! random number generator
real y(600)

c Counters =====
integer Np                     ! total number of particles
integer ix, jy, kz, itime      ! "bin" reference
integer i, n, tp, k, p, Pr     ! counters
integer isrc                   ! source counter
integer psrc                   ! number of sources
integer idum                   ! random # generator (-ve)

c Parameters =====
parameter (Ustar = 0.43)
parameter (Sc = 0.63)
parameter (kv = 0.4)
parameter (Zo = 0.054)
parameter (Co = 3.1)
parameter (deltaX = 0.3)
parameter (deltaY = 0.204)      ! laser 1 (102/500)
c parameter (deltaY = 0.426)      ! laser 2 (213/500)
parameter (deltaZ = 0.3)
parameter (hs = 0.5)

parameter (Xlsr = 24)           ! from source to laser 1
c parameter (Xlsr = 45)           ! from source to laser 2
parameter (hs = 0.5)
parameter (Zlsr = 1.5)
parameter (Zrflt = 7*Zo)       ! 7Zo, Zo
parameter (deltat = 5)

```

```

parameter (Co = 3.1)

parameter (psrc = 60)
parameter (Np = 1E+03)
parameter (Q = 4.65E-03)

c Output Stuff =====
character outfile*20
integer laser,run,last_run
laser = 1005
run = 301
last_run = 303
idum = -1000
c 1. CREATE OUTPUT FILE =====
do run = 301,last_run
  write(outfile,'(i4.4,','_',' ',i3.3)')laser,run
  open(3,file=outfile, status='unknown')
do jy = 1,500
  do itime = -1,64
    C(jy,itime)=0.0
    trez(jy,itime)=0.0
    tbar(jy,itime)=0.0
c      trez_new(jy,itime)=0.0
  end do
end do
p = 0
Pr = 0
write(*,*) 'Np =',Np,' ',outfile, ' '
sigmaW = 1.3*Ustar
sigmaV = 2*Ustar
sigmaU = 2*Ustar
k = 1
do jy = 1,500
  y(jy)=-100.0+(float(jy))*0.2
end do

c 2. START SOURCE AND PARTICLE LOOPS =====
write(*,*) 'Laser 1'
do isrc = 1, psrc
  tsrc = 5*(isrc - 0.5)
  do i=1,Np
    ru = gasdev(idum)    ! random number for u langevin eq.

```

```

rv = gasdev(idum)    ! random number for v langevin eq
rw = gasdev(idum)    ! random number for w langevin eq.

Xp = 0.0             ! Xp zero initially
Yp = 0.0             ! Yp zero initially
Zp = hs              ! source height
t = tsrc

Up = ru*sigmaU      ! initial U velocity
Vp = rv*sigmaV      ! initial V velocity
Wp = rw*sigmaW      ! initial W velocity

call traj(Zp,Yp,Up,tp,t,idum,i,isrc,Pr)

kz = int(Zp/deltaZ)
itime = int(tp/deltat)
c 3a). CATCH PARTICLES IN LASER =====
      if ((Zp.gt.(Zlsr - (0.5*deltaZ))).and.
          & (Zp.lt.(Zlsr + (0.5*deltaZ)))) then
          jy = int(Yp/deltaY)+375      ! laser 1
c          jy = int(Yp/deltaY)+256      ! laser 2
          itime = int(tp/deltat)
c 3b). COMPUTE RESIDENCE TIME OF PARTICLES IN LASER BINS =====
          if(jy.ge.0.and.jy.le.500) then
              p = p + 1
              if (Up.ne.0.) then
                  dtrez = 1/abs(Up)
                  trez(jy,itime) = trez(jy,itime) + dtrez
              else
                  dtrez = 1000.
                  trez(jy,itime) = trez(jy,itime) + dtrez
              end if
          end if
      end do ! next particle
end do ! next source

write(*,*) 'particles through laser:',p

c 4a). COMPUTE CONCENTRATION =====
do jy = 1,500
c    do itime = -1,32

```



```

        do itime = -1,64
            tbar(jy,itime)=trez(jy,itime)/(Np)
            C(jy,itime)=Q*tbar(jy,itime)/(deltaZ*deltaY)
c         write(*,*) 'CONC:',C(250,itime), itime
        end do
    end do

    do jy = 1,500
        C(jy,-1) = 0.0
        C(jy,64) = 0.0
    end do

c 4b). COMPUTE LINE AVG. CONCENTRATION =====
    call lineavg(C,itime,jy,meanC)
c     write(*,*) meanC

c 4c). COMPUTE 5 MIN AVERAGE =====
    call Five_min_avg(meanC,avg)
c     write(*,*) 'CONC:', avg

c 5. WRITE OUTPUT =====
c     do i=-1,32
        do i= -1,64
            if (i.eq.-1) then
                write(3,*) '# laser',laser,'with delay'
                write(3,*) '# run',run
                write(3,*) '# Np = ',Np
                write(3,*)
                write(3,*) '# Five minute average =',avg,'kg per m^3'
                write(3,*)
                write(3,*) '# t          C'
            endif
c         write(3,*) i/6.,meanC(i)
            write(3,*) i/12.,meanC(i)
        end do

        write(*,*) 'Five minute average =',avg,'kg per m^3'
        write(3,*) 'Particles Reflected:',Pr

100    format (i4,1h ,f20.15,1h ,f20.15,1h ,f20.15,1h ,i10)
        close(3)          ! close the file
    end do ! close run loop

```

```

      END
c-----
c          Subroutine to compute particle trajectories
c-----
      subroutine traj(Zp,Yp,Up,tp,t,idum,i,isrc,Pr)
      implicit none

c Reals =====
      real ran3, gasdev          ! for the random number generator
      real dxi_u,dxi_v,dxi_w     ! gaussian random numbers
      real Ustar                 ! Frictional velocity (m/s),
      real kv                    ! von Karman constant
      real Zo                    ! roughness length
      real Co                    ! universal constant

      real deltaX,deltaY,deltaZ  ! size of laser bins
      real Xlsr
      real Zrflt
      real Xp,Yp,Zp,Wp,Up,Vp     ! position/velocity
      real dZ,dX,dY,dW,dU,dV     ! position/velocity increments
      real b, e                  ! U, V, and W coefficients
      real au, av, aw
      real sigmaU, sigmaV, sigmaW ! velocity variances
      real meanU, Ubar, Vbar
      real Xprev
      real Tl_u, Tl_v, Tl_w      ! lagrangian time scale
      real dtu, dtv, dtw
      real dt,t                  ! time step
      real beta                  ! angle for mean wind direction
      real small_u, tao          ! surface-delay algorithm

c Counters =====
      integer i,isrc             ! counter for sources
      integer idum               ! must be negative
      integer k,flag(70), Pr
      integer tp

c Parameters =====
      parameter (Ustar = 0.43)
      parameter (kv = 0.4)
      parameter (Co = 3.1)
      parameter (Zo = 0.054)

```

```

parameter (deltaY = 0.2)           ! 500 bins of 0.2 m each
parameter (deltaX = 0.3)
parameter (Xlsr = 24)              ! distance from source to laser 1
c parameter (Xlsr = 45)            ! distance from source to laser 2
parameter (Zrflt = Zo)

parameter (beta = 5.7339302)      ! laser 1
c parameter (beta = 5.7793088)    ! laser 2
parameter (sigmaU = 2*Ustar)
parameter (sigmaV = 2*Ustar)
parameter (sigmaW = 1.3*Ustar)
parameter (tao=2.5*Zrflt/sigmaW)
c Progress Indicator =====
do k = 1,70
  flag(k) = 0
end do
c 1a). COMPUTE COEFFICIENTS FOR dX,dY,dZ,dU,dV,dW =====
do while (Xp.lt.Xlsr)

  dxi_u = gasdev(idum)
  dxi_v = gasdev(idum)
  dxi_w = gasdev(idum)

  Ubar = (Ustar/kv)*cos(beta)*alog(Zp/Zo)
  Vbar = (Ustar/kv)*sin(beta)*alog(Zp/Zo)

  small_u=((Ustar*Zo)/(kv*(Zrflt-Zo)))*((Zrflt/Zo)*
&      (alog(Zrflt/Zo))-(Zrflt/Zo)+1)

  e = (Ustar**3)/(kv*Zp)

  Tl_u = 2*(sigmaU**2)/(Co*e)
  Tl_v = 2*(sigmaV**2)/(Co*e)
  Tl_w = 2*(sigmaW**2)/(Co*e)

  au = -Up/Tl_u
  av = -Vp/Tl_v
  aw = -Wp/Tl_w

  b = (Co*e)**0.5

  dtu = 0.1*Tl_u

```

```

dtv = 0.1*TL_v
dtw = 0.1*TL_w

dt = min(dtu,dtv,dtw)
if (dt.eq.0.) dt = 1.0E-06
c 1 b). COMPUTE dX,dY,dW,dZ,dU,dV =====

dX = (Ubar + Up)*dt
dY = (Vbar + Vp)*dt
dZ = Wp*dt

Zp = Zp + dZ

c ----- progress indicator-----
if (i.eq.1.and.flag(isrc).eq.0) then
write(*,*) 'SOURCE:',isrc
c write(*,*) 'displacement=',(small_u*tao)
c write(*,*) 'time=',tao
flag(isrc) = 1
end if
c 2. COMPUTE TRAJECTORIES =====
if (Zp.le.Zrflt) then
Pr = Pr + 1
Wp = -Wp
Zp = (2*Zrflt)-Zp
c ----- surface delay algorithm -----
t = t + tao
Xp = Xp + (small_u*tao)
end if
c ----- trajectories -----
Xp = Xp + dX
Yp = Yp + dY

dW = (aw*dt) + (b*dxi_w)*sqrt(dt)
dU = (au*dt) + (b*dxi_u)*sqrt(dt)
dV = (av*dt) + (b*dxi_v)*sqrt(dt)

Up = Up + dU
Vp = Vp + dV
Wp = Wp + dW

t = t + abs(dt)

```

```

        tp = int(t)
    end do
    return
end

c-----
c      Subroutine to compute line-average concentrations
c-----
subroutine lineavg(C,itime,jy,meanC)

    implicit none
    integer i,jy,itime,N
    real meanC(-1:64)
    real C(500,-1:64)
    N = 64

    do i=-1,64
        meanC(i) = 0.0
    end do
    do itime = -1,64
        do jy = 1,500
            meanC(itime) = meanC(itime) + C(jy,itime)
        end do
        meanC(itime) = meanC(itime)/float(N)
    end do
    return
end

c-----
c      Subrouting to compute "5 min" averages
c-----
subroutine Five_min_avg(meanC,avg)

    implicit none
    integer i, N
    real meanC(-1:64)
    real avg
    N= 64
    avg = 0.0

    do i = -1,64
        avg = avg + meanC(i)
    end do
    avg = avg/float(N)

```

```

return
end
c-----
c      Subroutine to compute Gaussian Random Number, dxi
c-----
      FUNCTION gasdev(idum)
      INTEGER idum
      REAL gasdev
c      uses ran1 to return a normally distributed
c      deviate with zero mean and
c      unit variance.

      INTEGER iset
      REAL fac,gset,rsq,v1,v2,ran1
      SAVE iset,gset
      DATA iset/0/
      if (idum.lt.0) iset = 0
      if (iset.eq.0) then
1          v1 = 2.*ran3(idum)-1.
          v2 = 2.*ran3(idum)-1.
          rsq = v1**2+v2**2
          if (rsq.ge.1..or.rsq.eq.0.) goto 1
          fac = sqrt(-2.*log(rsq)/rsq)
          gset = v1*fac
          gasdev = v2*fac
          iset=1
      else
          gasdev = gset
          iset = 0
      endif
c      write(*,*) 'GASDEV:',idum
      return
      END
c
      FUNCTION ran3(idum)
      real ran3
c      portable random number generator
      parameter (mbig=1000000000,mseed=161803398,mz=0,fac=1.e-9)
      integer ma(55)
      save ma,inext,inextp,iff
      data iff /0/
c

```

```
if(idum.lt.0.or.iff.eq.0)then
  iff=1
  mj=mseed-iabs(idum)
  mj=mod(mj,mbig)
  ma(55)=mj
  mk=1
  do 11 i=1,54
    ii=mod(21*i,55)
    ma(ii)=mk
    mk=mj-mk
    if(mk.lt.mz)mk=mk+mbig
    mj=ma(ii)
11  continue
  do 13 k=1,4
    do 12 i=1,55
      ma(i)=ma(i)-ma(1+mod(i+30,55))
      if(ma(i).lt.mz)ma(i)=ma(i)+mbig
12  continue
13  continue
  inext=0
  inextp=31
  idum=1
endif
inext=inext+1
if(inext.eq.56)inext=1
inextp=inextp+1
if(inextp.eq.56)inextp=1
mj=ma(inext)-ma(inextp)
if(mj.lt.mz)mj=mj+mbig
ma(inext)=mj
ran3=mj*fac
RETURN
end
```

## Appendix 2

### Sensor Configurations Used for bLS Emission Estimates

Release Date	Configuration
Sept30	Lasers 5 and 6. $C_b$ forced to 2.03 ppm
	Lasers 5, 6 and NSA
	Lasers 5, 6, and 7. $C_b$ forced to 2.03 ppm
	Lasers 5, 6, 7 and NSA
	Sample Line with GC data. $C_b$ forced to 2.03 ppm
Oct2	Lasers 5 and 8. $C_b$ forced to 2.00 ppm
	Lasers 5, 3 and 8.
	Lasers 5 and 4. $C_b$ forced to 2.00 ppm
	Lasers 5, 4 and 8.
	Sample Line with GC data. $C_b$ forced to 2.00 ppm

Table 6.1: Details of the laser configurations used in the bLS emission estimates. Please refer to Fig. (4.6) to see the positions of the sensors around the farm. ‘NSA’ refers to the stand-alone laser unit located in the northernmost position away from the farm complex. ‘ $C_b$ ’ refers to the atmospheric background methane concentration. The first three configurations listed for the September 30th release, and the first two listed for the October 2nd release were used to obtain the results listed in Chapter 5.



# Bibliography

- Boadi, D., Witenberg, K., Scott, S., Burton, D., Buckley, K., Small, J., & Ominski, K. 2004, *Canadian Journal of Animal Sciences*, 445
- Brutsaert, W. 1982, *Evaporation into the Atmosphere: Theory, History and Applications* (Dordrecht, Netherlands: D. Reidel Publishing Company)
- Charlson, R. J. 1999, *Nature*, 401, 741
- Denmead, O., Harper, L., & Sharpe, R. 2000, *Agric. For. Meteorol.*, 104, 67
- Denmead, O. & Raupach, M. 1993, *ASA Special Publication*, 55
- Desjardins, R., Denmead, O., Harper, L., McBain, M., Mass, D., & Kaharabata, S. 2004, *Atmospheric Environment*, 38, 6855
- Desjardins, R., Kulshreshtha, S., Junkins, B., Smith, W., Grant, B., & Boehm, M. 2001, *Nutrient Cycling in Agroecosystems*, 60, 317
- Flesch, T. & Wilson, J. 1992, *Bound. Layer Meteorol.*, 61, 349
- Flesch, T., Wilson, J., Harper, L., Crenna, B., & Sharpe, R. 2004, *J. Appl. Meteorol.*, 43, 487
- Flesch, T. K., Wilson, J. D., Harper, L. A., & Crenna, B. P. 2005, *Atmospheric Environment*, 39, 4863

- Flesch, T. K., Wilson, J. D., & Yee, E. 1995, *J. Appl. Meteorol.*, 34, 1320
- Harper, L., Denmead, O., Freney, J., & Byers, F. 1999, *Canadian Journal of Animal Science*, 77, 1392
- Harvey, M., Brailsford, G., Bromley, A., Lassey, K., Mei, Z., Kristament, I., Reisinger, A., Walker, C., & Kelliher, F. 2002, *Atmospheric Environment*, 36, 4663
- Houghton, J., Filho, L. M., Bruce, J., Lee, H., Callander, B., Haites, E., Harris, N., & Maskell, K. 1995, *Climate Change 1994: Radiative Forcing of Climate Change and An Evaluation of the IPCC IS92 Emission Scenarios* (Cambridge: Cambridge University Press)
- Hsieh, C.-I., Katul, G. G., Schieldge, J., Sigmon, J. T., & Knoerr, K. K. 1997, *Water Resources Research*, 33, 427
- Johnson, K., Huyler, M., Westberg, H., Lamb, B., & Zimmerman, P. 1994, *Environmental Science and Technology*, 28, 359
- Judd, M. J., Kellier, F., Ulyatt, M., Lassey, K., Tate, K., Shelton, D., Harvey, M., & Walker, C. 1999, *Global Change Biology*, 5, 647
- Kaimal, J. & Finnigan, J. 1994, *Atmospheric Boundary Layer Flows* (Oxford: Oxford University Press), 289
- Kinsman, R., Sauer, R., Jackson, H., & Wolynetz, M. 1995, *J. Dairy Science*, 78, 2760
- Lassey, K. R., Ulyatt, M. J., Martin, R. J., Walker, C. F., & Shelton, I. D. 1997, *Atmospheric Environment*, 31, 2905
- Laubach, J. & Kelliher, F. M. 2005, *Agric. For. Meteorol.*, 129, 137

- Leuning, R., Baker, S., Jamie, I., Hsu, C., Klein, L., Denmead, O., & Griffith, D. 1999, *Atmospheric Environment*, 33, 1357
- Leuning, R., Denmead, O., Miyata, A., & Kim, J. 2000, *Agric. Forest Meteorol.*, 104, 233
- Marik, T. & Levin, I. 1996, *Glob. Biogeochem. Cycl.*, 10, 413
- Mathison, G. 1997, *Canadian Journal of Animal Science*, 77, 545
- Murray, R., Bryant, A., & Leng, R. 1976, *British Journal of Nutrition*, 36, 1
- Pearce, F. 1989, *New Scientist*, 6, 37
- Sommer, S., McGinn, S., Hao, X., & Larney, F. 2004, *Atmospheric Environment*, 38, 4643
- Thomson, D. 1987, *J. Fluid Mech.*, 180, 529,556
- Thomson, D. J. & Montgomery, M. R. 1994, *Atmospheric Environment*, Vol. 28, No. 12, 1981
- Tol, R. S., Heintz, R. J., & Lammers, P. E. M. 2003, *Climatic Change*, 57, 71
- van Ouwerkerk, E. 1993, *Methods for measuring ammonia emissions from animal housing* (Netherlands: DLO, Wageningen)
- Werner, C., Wyngaard, J., & Brantley, S. 2000, *Geophysical Research Letters*, 27, 2925
- Weubbles, D. J. & Hayhoe, K. 2001, *Earth-Science Reviews*, 57, 117
- Wilson, J. 2004, *J. Applied Meteorol.*, 43, 1392

Wilson, J., Catchpoole, V., Denmead, O., & Thurtell, G. 1983, *Agricultural Meteorol.*, 29, 183

Wilson, J. & Flesch, T. 1993, *J. Appl. Meteorol.*, 32, 1695

Wilson, J., Flesch, T., & D'Amours, R. 2001a, *J. Applied Meteorol.*, 40, 1422

Wilson, J., Flesch, T., & Harper, L. 2001b, *Agric. For. Meteorol.*, 107, 207

Wilson, J. & Sawford, B. 1996, *Bound. Layer Meteorol.*, 78, 191